HHS Public Access

Author manuscript

Neuron. Author manuscript; available in PMC 2019 April 04.

Published in final edited form as:

Neuron. 2018 April 04; 98(1): 127–141.e7. doi:10.1016/j.neuron.2018.03.008.

Rbfox1 Regulates Synaptic Transmission Through the Inhibitory Neuron Specific vSNARE Vamp1

Celine K. Vuong[1,6], **Weizheng Wei**[2], **Ji-Ann Lee**[3], **Chia-Ho Lin**[4], **Andrey Damianov**[4], **Luis de la Torre-Ubieta**[5], **Reem Halabi**[4], **Klara Olofsdotter Otis**[3,7], **Kelsey C. Martin**[3], **Thomas J. O'Dell**[2], and **Douglas L. Black**[4,8,*]

[1]Molecular Biology Interdepartmental Doctoral Program, University of California, Los Angeles, Los Angeles, CA 90095, USA

[2]Department of Physiology, David Geffen School of Medicine, University of California, Los Angeles, Los Angeles CA, 90095, USA

[3]Department of Biological Chemistry, David Geffen School of Medicine, University of California, Los Angeles, Los Angeles CA, 90095, USA

[4]Department of Microbiology, Immunology and Molecular Genetics, David Geffen School of Medicine, University of California, Los Angeles, Los Angeles CA, 90095, USA

[5]Department of Psychiatry and Biobehavioral Sciences, David Geffen School of Medicine, University of California, Los Angeles, Los Angeles CA, 90095, USA

[6]Molecular Biology Institute, University of California, Los Angeles, Los Angeles, CA 90095, USA

Summary

Dysfunction of the neuronal RNA binding protein RBFOX1 has been linked to epilepsy and autism spectrum disorders. Rbfox1 loss in mice leads to neuronal hyper-excitability and seizures, but the physiological basis for this is unknown. We identify the vSNARE protein Vamp1 as a major Rbfox1 target. Vamp1 is strongly downregulated in *Rbfox1 Nes-cKO* mice due to loss of 3′ UTR binding by Rbfox1. Cytoplasmic Rbfox1 stimulates Vamp1 expression in part by blocking *microRNA-9*. We find that Vamp1 is specifically expressed in inhibitory neurons, and that both *Vamp1* knockdown and *Rbfox1* loss lead to decreased inhibitory synaptic transmission and E/I imbalance. Re-expression of Vamp1 selectively within interneurons rescues the electrophysiological changes in the Rbfox1 cKO, indicating that Vamp1 loss is a major contributor

*Correspondence: DougB@microbio.ucla.edu.

[7]Present address: Sainsbury Wellcome Centre for Neural Circuits and Behaviour, Gower Street, London, WC1E 6BT, UK.

[8]Lead Contact

Declaration of Interests

The authors declare no competing interests.

Author Contributions

Conceptualization, C.K.V., D.L.B. and T.J.O; Software, C.H.L; Formal Analysis, C.K.V., W.W., T.J.O., C.H.L. and L.T.U.; Investigation, C.K.V., W.W., R.H. and L.T.U.; Resources, J.A.L. and A.D.; Writing – Original Draft, C.K.V. and D.L.B.; Writing – Review & Editing, all authors; Funding Acquisition, C.K.V., J.A.L., K.C.M., T.J.O. and D.L.B.

to the *Rbfox1 Nes-cKO* phenotype. The regulation of interneuron-specific Vamp1 by Rbfox1 provides a paradigm for broadly expressed RNA-binding proteins performing specialized functions in defined neuronal subtypes.

eTOC

Regulation of Vamp1 expression in inhibitory neurons by cytoplasmic Rbfox1 is required for proper inhibitory synaptic transmission and E/I balance. Restoring Vamp1 levels in Rbfox1 cKO inhibitory neurons is sufficient to rescue physiological defects.

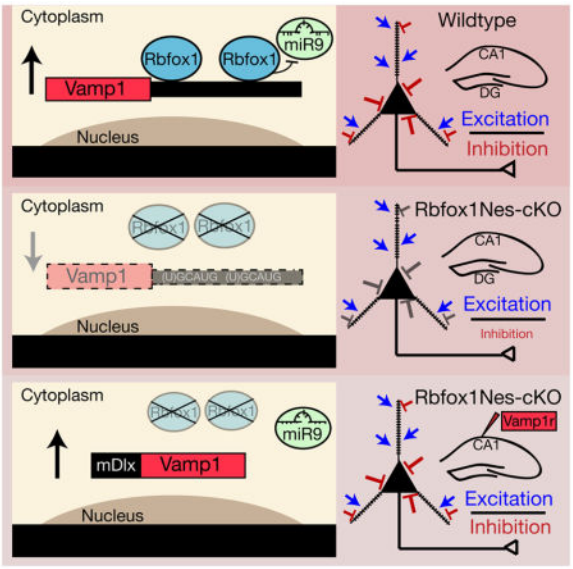

Keywords

E/I balance; inhibitory synaptic transmission; Vamp1; Rbfox1; RNA-binding protein; posttranscriptional regulation; microRNA-9

Introduction

The importance of post-transcriptional gene regulation in neuronal function has been underscored by the many RNA binding proteins (RBP) linked to neurodevelopmental and neurologic disorders (Chabot and Shkreta, 2016; Licatalosi and Darnell, 2006; Poulos et al., 2011; Srikantan and Gorospe, 2012). RBPs function in many critical cellular processes including alternative splicing, mRNA decay, translation and subcellular mRNA localization. However, an understanding of how RBPs determine specific physiological changes in particular cell types has not been achieved. These RBPs are often broadly expressed throughout the brain and present pleiotropic phenotypes in knockout mice, reflecting many splicing and gene expression changes. The functions of these extensive post-transcriptional regulatory programs and their roles in specific neuronal cell types and circuits are still largely unexplored.

The Rbfox family of brain-enriched RBPs is widely studied as regulators of alternative splicing. The three mammalian family members – Rbfox1, Rbfox2 and Rbfox3 – each has a highly conserved RNA recognition motif (RRM) that binds the sequence (U)GCAUG (Conboy, 2017; Jin et al., 2003; Kuroyanagi, 2009; Ponthier et al., 2006; Underwood et al., 2005). In regulating splicing in the nucleus, Rbfox proteins bind to pre-mRNAs within a Large Assembly of Splicing Regulators (Damianov et al., 2016; Ying et al., 2017). Rbfox transcripts are themselves alternatively spliced to create cytoplasmic isoforms that bind within 3′ UTR sequences to regulate translation (Carreira-Rosario et al., 2016; Lee et al., 2016). The ratio of nuclear to cytoplasmic Rbfox varies between cells and can be dynamically regulated by membrane depolarization (Lee et al., 2009).

Previous work found that pan-neuronal *Rbfox1*$^{loxP/loxP}$ *; Nestin-Cre*$^{+/-}$ knockout mice (*Rbfox1 Nes-cKO*) were susceptible to spontaneous and induced seizures (Gehman et al., 2011). Extracellular recordings in the dentate gyrus of the hippocampus found that low intensity presynaptic fiber stimulation elicited larger field EPSPs in the cKO compared to wildtype. Spine density and expression levels of the synaptic proteins such as Synapsin-I and PSD-95 were unchanged, suggesting that a change in synaptic function rather than synapse number was responsible for neuronal hyper-excitability in the *Rbfox1 Nes-cKO* brain. Whole transcriptome profiling by microarray and RNA-seq identified multiple gene expression and alternative splicing changes in the knockout mice, but these were assayed in whole brain and difficult to relate to the electrophysiological results (Gehman et al., 2011; Lovci et al., 2013; Weyn-Vanhentenryck et al., 2014).

Recent work demonstrated a role for cytoplasmic Rbfox1 in promoting mRNA stability and/or translation by binding the 3′UTRs of target transcripts (Carreira-Rosario et al., 2016; Lee et al., 2016). This cytoplasmic portion of the Rbfox1 regulatory program was enriched for many key neuronal functions such as the calcium signaling pathway, as well as regulatory modules controlling cortical development and modules altered in ASD (Lee et al., 2016). Interestingly, this cytoplasmic program largely affected transcripts different from those regulated by the splicing program. Thus, loss of cytoplasmic Rbfox1 likely also contributes to the pathophysiology of the *Rbfox1 Nes-cKO* in parallel with the splicing changes controlled by the nuclear protein. However, the specific contribution of the cytoplasmic Rbfox1 to altered neuronal excitability remains unexplored. Here we examine the changes in gene expression and electrophysiology controlled by Rbfox1, specifically in the hippocampus. We identify the vSNARE *Vamp1* as a major target of cytoplasmic Rbfox1 that plays a critical role in inhibitory synaptic transmission. Our results demonstrate how regulation of Vamp1 mRNA abundance by cytoplasmic Rbfox1 controls synaptic function in a specific neuronal cell type and contributes to the greater network defects in the *Rbfox1 Nes-cKO* brain.

Results

Vamp1 is a direct Rbfox1 target

To obtain a more refined view of posttranscriptional regulation specifically by Rbfox1 and specifically in the hippocampus, we performed RNA-seq on adult (P60–70) hippocampi isolated from *Rbfox1 Nes-cKO* and wildtype littermates (n=3 each genotype). We identified

significant changes in both alternative splicing and overall mRNA abundance, consistent with the dual role of Rbfox1 in regulation of alternative splicing and mRNA stability. As seen previously, Rbfox1-dependent gene expression changes did not significantly overlap with splicing changes (19 genes changing in both overall mRNA abundance and exon usage, Figure S1A and Table S3) (Lee et al., 2016). The gene expression changes identified in the cKO hippocampus (1034 genes) partially overlapped (183 genes) with previously identified cytoplasmic Rbfox1 targets in cultured neurons (774 genes) (Lee et al., 2016). The differences between these RNAseq datasets are likely due both to gene expression changes between tissue and *in vitro* culture, to differences between prolonged versus acute loss of Rbfox, and to the additional depletion of Rbfox3 in the previous study.

Focusing on the 1034 differentially expressed (DE) genes detected in the hippocampus, we examined the overlap of our target transcripts with Rbfox1 iCLIP datasets from the soluble nucleoplasmic fraction of adult mouse forebrain (Damianov et al., 2016) and from the cytoplasmic fraction of cultured primary neurons (Lee et al., 2016). We filtered the target list by requiring DE genes to contain 3′UTR CLIP clusters in both the nucleoplasmic and cytoplasmic datasets, and that these clusters also contain an Rbfox motif [(U)GCAUG] within ±10 nucleotides of the edge of the cluster (Figure 1A). These stringent filters generated a list of 15 high confidence genes directly regulated by Rbfox1 (Figure 1B and Table S4), and included adenylyl cyclase, potassium channels, neuropeptide Y and others. Most targets were downregulated upon Rbfox1 loss, as seen previously in cultured neurons, but four were upregulated and thus appear to be repressed by the protein. Using less stringent filters, many additional transcripts are seen to be regulated by Rbfox1 (Tables S2 and S4).

Vamp1 (also known as *Synaptobrevin1*) mRNA exhibited one of the largest changes in expression, decreasing by 50% in the *Rbfox1 Nes-cKO* hippocampus as measured by RNA-seq and quantitative PCR (qPCR) (Figure 1B, D). RBFOX1 binding to the Vamp1 mRNA is restricted to the 3′UTR and is observed in the nucleoplasmic and cytoplasmic fractions, but not in the high molecular weight, chromatin-associated nuclear pellet where the Rbfox1 protein binds within introns to regulate splicing (Damianov et al., 2016) (Figure 1C). Immunoblotting for Vamp1 in cKO and wildtype adult brains, we found that Vamp1 protein, like the mRNA, was dramatically depleted by ~80% in the cKO cortex and hippocampus (Figure 1E). Interestingly, there was relatively little effect on Vamp1 expression in the cerebellum, where its regulation presumably involves additional factors (Figure 1D, E). The mRNA and protein levels of the paralog Vamp2 were unchanged between *Rbfox1 Nes-cKO* and wildtype (Figure S1F, G). In the forebrain, the reduced Vamp1 mRNA and protein levels and the direct binding of RBFOX1 to the Vamp1 3′UTR suggest a role for cytoplasmic Rbfox1 in regulating Vamp1 expression by promoting its mRNA stability and/or translation.

The Vamp1 3′UTR confers Rbfox1-dependent expression

Despite RBFOX1 binding to the *Vamp1* 3′UTR, it was possible that the decreased Vamp1 expression in the cKO forebrain resulted from loss of nuclear Rbfox1 function or from indirect effects of Rbfox1 loss. To assess the mechanisms of Rbfox1-mediated regulation, we cultured primary hippocampal neurons from *Rbfox1 Nes-cKO* embryos that lack both

the nuclear and cytoplasmic isoforms. Both Vamp1 mRNA and protein levels were reduced in cultured cKO neurons compared to the wildtype (Figure 2A), similar to the reduction observed in the adult cKO hippocampus (Figure 1D, E). Using adeno-associated virus (AAV) to re-express cytoplasmic Rbfox1 under the control of the human *Synapsin1* (*hSyn*) promoter in the cKO neurons, we found that this can rescue both Vamp1 mRNA and protein to levels comparable to wildtype neurons (C rescue; Figure 2A). These results demonstrate that cytoplasmic Rbfox1 is sufficient to promote Vamp1 expression. Given the observed binding in the *Vamp1* 3′UTR (Figure 1C), Rbfox1 may enhance Vamp1 mRNA stability or translation.

To examine the role of the *Vamp1* 3′ UTR in Rbfox1 regulation, we used the luciferase reporter system in primary hippocampal neurons (Figure 2B). For a reporter containing the full length *Vamp1* 3′UTR, Rbfox1 loss decreased expression by ~50% (FL, Figure 2C–D). Thus, expression from transcripts containing the *Vamp1* 3′UTR is strongly Rbfox1-dependent, with the residual expression possibly due to the presence of cytoplasmic Rbfox3 ((Lee et al., 2016); and see below). We tested the roles of the seven Rbfox binding motifs (U)GCAUG in stimulating expression by mutating them to (U)G*ACGU*. Mutation of the first six sites significantly reduced reporter expression (FLm1-6, Figure 2C–D), while mutation of all sites virtually abolished reporter expression (FLm1-7, Figure 2C–D). Notably, mutation of only the 3′-most Rbfox binding site reduced reporter expression as strongly as mutation of all six upstream sites (FLm7, Figure 2C–D). We did not observe a significant change in expression of the FLm1-6 mutant upon loss of Rbfox1. In contrast, there was a visible, though not statistically significant, decrease in FLm7 reporter expression with loss of Rbfox1. These different responses to the loss of Rbfox1 by the mutant 3′ UTRs may result from differences in their responses to cytoplasmic Rbfox3 (Lee et al., 2016). Overall, these results indicate that RBFOX1 binding to the *Vamp1* 3′UTR strongly stimulates its expression and that the 3′-most Rbfox binding site plays a major role in this regulation.

We noted that the 3′-most Rbfox binding site immediately abuts a microRNA response element (MRE) identified by TargetScan as a binding site for *microRNA-9* (MiR-9 MRE, magenta; Figure 2E) (Friedman et al., 2009; Grimson et al., 2007; Lewis et al., 2005). The sequence encompassing these two regulatory elements shows a high degree of mammalian conservation (Figure 2E), indicating a likely regulatory function. We hypothesized that RBFOX1 binding to the 3′-most GCAUG contributes to stabilization of the Vamp1 transcript by blocking *miR-9* binding. To dissect the roles of this GCAUG and the adjacent *miR-9* site, we created a luciferase reporter containing a fragment of the *Vamp1* 3′UTR that includes the last two Rbfox binding sites and the *miR-9* site (3′F; Figure 2E). Luciferase expression from this reporter was again dependent on Rbfox1, with a 40% reduction in the cKO neurons compared to wildtype (3′F, red bar; Figure 2F). Similar to the full-length 3′UTR, mutating the final GCAUG in this fragment dramatically decreased reporter expression (3′Fm7, black bar; Figure 2F). Conversely, mutation of the *miR-9* MRE increased expression in wildtype neurons (3′F vs 3′FmiR9m, black bars; Figure 2F) and reduced the effect of Rbfox1 loss in the cKO neurons (3′F vs. 3′FmiR9m, red bars; Figure 2F). A compound mutation of the *miR-9* MRE and both GCAUG elements (3′Fm6-7miR9m; Figure 2F) increased reporter expression relative to mutation of only the

3′-most Rbfox site (3′Fm7 vs 3′Fm6-7miR9m, black bars; Figure 2F). These results indicate that *miR-9* is repressive of Vamp1 expression and that this repression is overcome by RBFOX1 binding. The enhancing effect of the upstream sites indicate that RBFOX binding can also stimulate expression on its own.

To confirm *miR-9* targeting of the *Vamp1* 3′UTR, we used AAV to deliver a Tough Decoy (TuD) (Bak et al., 2013; Haraguchi et al., 2009; Xie et al., 2012) containing sequence complementary to the mature *miR-9* or a control sequence (Figure 2G). We observed ~50% reduction of mature *miR-9* levels in neurons transduced with the inhibitor (TuD-miR9) compared to control (TuD-ctrl) (Figure 2G). We then tested the effect of *miR-9* inhibition on the expression of the FL and FLm7 reporters. Suppressing *miR-9* in the presence of Rbfox1 did not significantly change expression of the FL reporter, indicating that RBFOX1 binding at the 3′ end of the UTR efficiently blocks *miR-9* activity (FL, black vs orange bars; Figure 2H). In cKO neurons with this luciferase reporter, inhibition of *miR-9* resulted in a visible, though not statistically significant, increase in expression compared to the control TuD (FL, red vs blue bars; Figure 2H). Notably, the results were different with the FLm7 reporter containing a mutated Rbfox binding site adjacent to the *miR-9* MRE. For this construct, inhibition of *miR-9* significantly increased reporter expression in the presence of Rbfox1, indicating that loss of the 3′most Rbfox binding site renders the reporter responsive to *miR-9* (FLm7, orange vs black bars; Figure 2H). A similar increase in FLm7 expression with *miR-9* inhibition was seen in the cKO neurons (FLm7, blue bar; Figure 2H), but did not reach statistical significance. Overall, these results indicate that RBFOX1 binding to the upstream sites promotes expression independently of *miR-9*, while the 3′-most Rbfox site is blocking the effect of *miR-9*.

Vamp1 is specifically expressed in inhibitory neurons

V*amp1* (*Synaptobrevin1/Syb1*) is a paralog of the well-studied vSNARE *Vamp2* (*Synaptobrevin2/Syb2*), which is found in both excitatory and inhibitory neurons and is critical for synaptic vesicle docking and neurotransmitter release (Deák et al., 2006; Schoch et al., 2001). Although much less characterized, VAMP1 is highly homologous to VAMP2 in protein sequence and domain structure (Figure 3A), and several studies have demonstrated that Vamp1 functions similarly to Vamp2 in regulating synaptic vesicle release (Liu et al., 2011; Zimmermann et al., 2014). We observed that both proteins are expressed in the adult mouse brain, although the onset of VAMP1 expression occurs quite late in development (P15), well after the induction of VAMP2 (E18; Figure 3B). In primary hippocampal neurons, anti-VAMP1 antibodies yielded the punctate staining pattern expected from a pre-synaptic protein. Virtually all VAMP1$^+$ puncta also contained VAMP2, though only a subset of VAMP2 puncta were positive for VAMP1 (~20% Vamp2$^+$/Vamp1$^+$; Figure 3C). The late induction of VAMP1 expression *in vivo* and its restricted expression in cultured neurons suggested that Vamp1 is specifically expressed in a particular neuronal cell type. Indeed, Vamp1 has been reported to be preferentially expressed at inhibitory synapses (Ferecskó et al., 2015).

To examine Vamp1 expression in neuronal subtypes, we first performed double-label immunocytochemistry of Vamp1 and markers of excitatory and inhibitory neurons in

primary hippocampal cultures. Using Gad67 as an inhibitory pre-synaptic marker, we counted all puncta that were VAMP1$^+$ or GAD67$^+$, or were VAMP1$^+$/GAD67$^+$ double positive to obtain the total number of puncta. We found that over 80% of the total puncta counted were VAMP1$^+$/GAD67$^+$. In a parallel analysis, Vamp1 had virtually no overlap with the excitatory markers Vglut1 and Vglut2 (Figure 4A, B). We observed a similar co-localization with inhibitory markers in sections of adult mouse hippocampi. VAMP1$^+$ puncta were enriched perisomatically in the CA1 and CA3 pyramidal layers (s.p.), and in the dentate granule (DG) layer. VAMP1$^+$ puncta were also detected more sparsely in stratum oriens (s.o.) and radiatum (s.r.) of CA1 and CA3, as well as the DG molecular layer and hilus (Figure 4C–F, Figure S3 B–E, and data not shown). Over 85% of puncta within the CA1 s.p. were VAMP1$^+$/GAD67$^+$ (Figure 4C,D). Notably, co-localization was significantly reduced in the *Rbfox1 Nes-cKO*, where ~50% of puncta were now GAD67$^+$/VAMP1$^-$. VAMP1 similarly co-localized with GAD67 in s.o. and s.r. (~80%), with a similar reduction in the *Rbfox1 Nes-cKO* (~30%) (Figure 4D). Rbfox1 loss led to a significant reduction in the number of detectable VAMP1$^+$ puncta in all hippocampal regions assayed (Figure S3A). Given the reduced VAMP1 levels observed by immunoblot, reduced VAMP1 co-localization with GAD67 in the cKO hippocampus is likely due to a loss of VAMP1$^+$ puncta rather than to mislocalization of the protein. The high level of co-localization between VAMP1$^+$ and GAD67$^+$ puncta confirmed our initial immunocytochemical observations that Vamp1 is expressed specifically in GABAergic inhibitory neurons. VAMP1 co-localization with GAD67 is also consistent with the perisomatic enrichment of VAMP1$^+$ puncta in the pyramidal layers, an innervation pattern typical of Parvalbumin-expressing (PV$^+$) basket cells (Tremblay et al., 2016).

We found that VAMP1 co-localized well with both PV (data not shown) and Synaptotagmin2 (SYT2), a marker of PV$^+$ interneuron pre-synaptic terminals (Sommeijer and Levelt, 2012) (Figure 4E,F). Comparable to our results with Vamp1 and Gad67, we observed a high degree of VAMP1 and SYT2 co-localization in the CA1 s.p. (over 85% of the total puncta were VAMP1$^+$/SYT2$^+$ double positive), s.o. and s.r. (~80%; Figure 4E, F). The *Rbfox1 Nes-cKO* hippocampus again showed a significant loss of VAMP1 immunoreactivity in SYT2$^+$ puncta (~40%, s.p. and ~30%, s.o. and s.r.; Figure 4E, F) due to a reduction in the number of VAMP1$^+$ puncta (Figure S3A). The presence of VAMP1$^+$ puncta in s.o. and s.r. of CA1 and the DG hilus, where VIP$^+$ and SST$^+$ interneurons are known to synapse, indicates that Vamp1 is likely also expressed in these cells. This consistent with the small number of VAMP1$^+$/SYT2$^-$ puncta observed in these areas.

One potential explanation for the reduction in VAMP1$^+$ puncta is a loss of inhibitory pre-synaptic sites. To address this possibility, we quantified the number of total SYT2$^+$ puncta per square micron in adult hippocampal sections to obtain an average Syt2 density. We found no significant difference in Syt2 puncta density in the s.p., s.o. or s.r. of CA1 between wildtype and *Rbfox1 Nes-cKO* hippocampi (Figure S5A), suggesting that the number of PV$^+$ pre-synaptic sites was not changed. This result indicated that the loss of VAMP1$^+$ puncta was due to a loss of Vamp1 expression rather than that of inhibitory pre-synaptic sites. We also assessed whether the excitatory or inhibitory synapse density was altered with loss of Rbfox1. Using co-localization of the respective pre- and post-synaptic excitatory markers Synaptophy-sin and PSD-95 in wildtype and cKO cultured neurons, we found no significant

difference in excitatory synapse density (Figure S5B). Similarly, using co-localization of pre-synaptic Gad65/67 and post-synaptic Gephyrin, we observed that inhibitory synapse density was also unchanged between the two genotypes (Figure S5C). Overall, our immunohistochemical results demonstrate that Vamp1 is expressed specifically in GABAergic inhibitory neurons, including at PV^+ pre-synaptic terminals in the hippocampus and likely also SST^+ and VIP^+ neurons. Additional co-localization of VAMP1 with SYT2 in the cortex and thalamus is presented in Figure S4 A–H. In the *Rbfox1 Nes-cKO* hippocampus, we observed significant reduction in the number of $VAMP1^+$ puncta at PV^+ pre-synaptic terminals but found no significant changes in total excitatory or inhibitory synapse density between wildtype and cKO hippocampal primary neurons. Thus, the decreased Vamp1 expression in the *Rbfox1 Nes-cKO* mice is expected to impair inhibitory synaptic transmission and in turn contribute to the hyperexcitation phenotype.

The Rbfox1 Nes-cKO hippocampus exhibits altered synaptic transmission

To examine whether inhibitory synaptic transmission is affected in the *Rbfox1 Nes-cKO* brain, we recorded miniature inhibitory (mIPSCs) and excitatory (mEPSCs) post-synaptic currents from CA1 and the DG in acute hippocampal slices from adult (P60–70) *Rbfox1 Nes-cKO* and wildtype littermates. The average mIPSC and mEPSC peak amplitudes were not significantly different between the two genotypes (Figure 5B, E and 5H, K). While mEPSC amplitudes appeared more variable in the cKO CA1 compared to WT (Figure 5A), this difference did not reach statistical significance. Interestingly, we found that the frequency of both mIPSC and mEPSC was significantly reduced in both CA1 and the DG (Figure 5C, F and 5I, L). The reduced mIPSC frequency is in concordance with a change in inhibitory synaptic transmission resulting from loss of Vamp1. The decrease in excitatory synaptic transmission is likely due in part to dysregulation of other Rbfox1 targets in excitatory cells (Gehman et al., 2011; Lee et al., 2016) but may also result from a compensatory, homeostatic response to the depletion in Vamp1 (see below). The reduced mIPSC frequency coupled with our finding that inhibitory synaptic density is unaffected in the cKO (Figure S5) are consistent with Vamp1 being an inhibitory-specific pre-synaptic protein with known roles in regulating release probability.

We next examined how the reduced frequency of both mIPSCs and mEPSCs might account for the neuronal hyper-excitability and seizures previously observed in the *Rbfox1 Nes-cKO* brain. To assess the excitation/inhibition (E/I) ratio in synaptic responses elicited by Schaffer collateral stimulation, we recorded synaptic currents in CA1 pyramidal cells voltage-clamped at −68mV and +10mV to isolate the respective excitatory AMPAR-mediated and the inhibitory $GABA_AR$-mediated currents (Figure 5M). Comparing the peak amplitudes of each component to obtain an E/I ratio, we found that while both mIPSC and mEPSC frequency are reduced in the *Rbfox1 Nes-cKO*, the E/I ratio of cKO neurons is increased relative to wildtype (Figure 5N). These results indicate that changes in synaptic transmission, rather than differences in excitatory or inhibitory synapse number, result in skewing of the E/I ratio towards increased excitation in the *Rbfox1 Nes-cKO* hippocampus, possibly due to the loss of Vamp1 in inhibitory neurons.

Vamp1 knockdown reduces inhibitory synaptic transmission

To assay functional changes resulting from the depletion of Vamp1 specifically, we used AAV delivery of shRNA to knock down *Vamp1* in primary hippocampal neurons and measured the amplitude and frequency of mIPSCs and mEPSCs. Compared to the control (shLuc), the Vamp1 knockdown neurons exhibited decreased mIPSC frequency (~50% decrease in shVamp1 compared to shLuc; Figure 6E) but no changes in amplitude (Figure 6D). Importantly, mIPSC frequency was fully restored in the Vamp1 knockdown by co-transduction of a virus expressing an shRNA-resistant *Vamp1* driven by the inhibitory neuron specific *mDlx* enhancer (Dimidschstein et al., 2016) (shVamp1 +mDlx-Vamp1r; Figure 6E). This re-expressed Vamp1 localized to axons in discrete puncta, similar to the pattern we observed in wildtype neurons, although the strong expression driven by the *mDlx* enhancer also led to VAMP1^{+} puncta in the dendrites (Figure S6G). These results confirmed the specificity of our *Vamp1* shRNA and indicated that the loss of Vamp1 leads to reduced mIPSC frequency in concordance with its role in inhibitory synaptic transmission. There was no significant change in mEPSC amplitude with Vamp1 knockdown (Figure 6G). Interestingly, we also observed a reduction in mEPSC frequency upon Vamp1 knockdown (~50% reduction in shVamp1 compared to shLuc; Figure 6H), and this could also be rescued by the inhibitory neuron specific re-expression of Vamp1 (shVamp1 +mDlx-Vamp1r; Figure 6H). This indicates that the initial reduction in mEPSC frequency upon Vamp1 loss likely resulted from a compensatory, homeostatic change in excitatory synaptic transmission in response to decreased inhibition (Fu et al., 2011; Qiu et al., 2012; Turrigiano, 2011). Overall, the Vamp1 knockdown and cell-type specific rescue show that Vamp1 is important for inhibitory synaptic transmission. The similarity of the electrophysiological changes resulting from Vamp1 depletion to those in the *Rbfox1 Nes-cKO* indicates that loss of Vamp1 expression plays a major role in the altered synaptic transmission observed in the cKO brain.

Vamp1 re-expression rescues synaptic transmission defects in the Rbfox1 cKO

To directly test whether reduced Vamp1 levels contribute to altered inhibitory synaptic transmission in the *Rbfox1 Nes-cKO* brain, we used stereotaxic delivery of AAV expressing *mDlx*-driven Vamp1 to adult wildtype and cKO hippocampi. *Nes-cKO* animals received bilateral injections of a control or rescue virus into each hippocampus. Wildtype littermates were injected with the tRFP-only virus in one hippocampus (Figure 7A). We observed no changes in synaptic transmission between injected and uninjected wildtype hippocampi (Figure S7 C–H). Inhibitory neuron-specific expression by the *mDlx* enhancer *in vivo* was previously demonstrated (Dimidschstein et al., 2016), and confirmed in our experiments by immunohistochemistry. We observed that *mDlx*-driven tRFP^{+} soma co-localized completely with GAD67^{+} cells, and that a large subset of these were also PV^{+} (Figure S7A). Generating acute slices of control and experimental hippocampi, we recorded mEPSCs and mIPSCs from CA1 across all three injected conditions. Comparing wildtype and cKO mice injected with control virus, we observed no changes in mEPSC or mIPSC amplitude (Figure 7D, G), but found a significant reduction in both excitatory and inhibitory current frequency (Figure 7E, H), similar to our previous observations (Figure 5). Comparing control and Vamp1 rescue cKO samples, we found, remarkably, that re-expression of Vamp1 in Rbfox1 knockout inhibitory neurons could rescue the reduction in mIPSC frequency to levels similar

to that of wildtype (Figure 7E). Interestingly, we also observed a rescue of mEPSC frequency with re-expression of Vamp1 in inhibitory neurons (Figure 7H). Confirming our results in rescuing Vamp1 knockdown in cultured neurons, this indicates that excitation is likely reduced in the Rbfox1 cKO hippocampus as a homeostatic response to loss of inhibition (Figure 6). These results demonstrate that simply increasing Vamp1 expression is sufficient to rescue the alterations in synaptic transmission observed in the pan-neuronal *Rbfox1 Nestin-cKO* hippocampus.

Discussion

We have examined how changes in mRNA metabolism controlled by an RNA binding protein can alter neurophysiology. Through its interactions with Vamp1, Rbfox1 can specifically regulate inhibitory synaptic transmission. While Rbfox1 is broadly expressed across many neuronal cell types, inhibitory neuron dependence on Vamp1 expression renders this neuronal population susceptible to Rbfox1 loss. This work demonstrates how the dysregulation of a broadly expressed RNA binding protein can result in defects in specific neuronal subtypes to alter neural circuit function.

Rbfox1, Vamp1 and inhibitory synaptic transmission

Through binding within 3′ UTR's, cytoplasmic Rbfox1 can increase target mRNA levels by promoting mRNA stability, antagonizing microRNA action or directly stimulating translation (Carreira-Rosario et al., 2016; Lee et al., 2016). We find that in the regulation of Vamp1, Rbfox1 appears to both antagonize microRNA action and directly increase expression. *Mi-croRNA-9* has largely been studied in the context of progenitor cell commitment to the neuronal lineage (Coolen et al., 2013; Delaloy et al., 2010; Sun et al., 2013; Yoo et al., 2011; Zhao et al., 2009). However, *miR-9* continues to be expressed in the adult brain (Liu et al., 2012), and recent work indicates that it plays important roles in mature neuronal function including dendritic arborization, and learning and memory (Dajas-Bailador et al., 2012; Giusti et al., 2014; Malmevik et al., 2016; Shi et al., 2013; Sim et al., 2016; Xue et al., 2016). Although both are broadly expressed across multiple neuronal cell types and brain regions, our work defines roles for Rbfox1 and *miR-9* in modulating the expression of Vamp1 specifically in inhibitory neurons. It will be interesting to further characterize the overlap in the Rbfox1 and *miR-9* regulatory networks and to understand the role of these opposing regulators in the function of other neuronal cell types and circuits.

The specific expression of Vamp1 in inhibitory neurons of the hippocampus and cortex indicates that these cells maintain a specific machinery for inhibitory synaptic transmission. Unlike excitatory neurons, which express only Vamp2, inhibitory neurons express both Vamp1 and Vamp2 (Figure 3C). Co-expression of Vamp1 and Vamp2 has also been observed at the neuromuscular junction (NMJ). Work examining NMJ function in a *Vamp1* hypomorphic mouse (*lew*/*lew*) (Nystuen et al., 2007) showed that loss of Vamp1 in motor neurons reduced the Ca^{2+} sensitivity and cooperativity of synaptic transmission. Vamp1 loss did not abolish neurotransmitter release, but reduced release probability, thus increasing the variability of the post-synaptic response (Liu et al., 2011). Like the NMJ, inhibitory synapses exhibit high neurotransmitter release probability in response to excitatory signaling

(Atallah and Scanziani, 2009; Pouille and Scanziani, 2001). Inhibitory neurons, in particular fast spiking PV^+ basket cells, play a pivotal role in the generation of cortical and hippocampal network oscillations through the precise control of principal cell firing (Bartos et al., 2007; Buzsáki and Wang, 2012; Cardin et al., 2009). These oscillations require the fast and precise conversion of excitatory input into inhibitory neurotransmitter release in PV^+ interneurons (Atallah and Scanziani, 2009; Hu et al., 2014; Jonas et al., 2004; Pouille and Scanziani, 2001). Although not statistically significant, we did observe an increase in mIPSC amplitude variability in the cKO hippocampus that may stem from reduced levels of Vamp1. Similar to its action in motor neurons, Vamp1 may increase release probability in the PV^+ neurons of the central nervous system and ensure the reliability of inhibitory synaptic transmission.

A dynamic interplay between Rbfox1 and *miR-9* may serve to fine tune inhibitory synaptic transmission during physiologically relevant states such as learning and memory. Gamma oscillations in the hippocampus driven by the precisely timed firing of PV^+ interneurons have been proposed to function in working memory, spatial processing and coordination across brain structures (Buzsáki and Wang, 2012; Colgin et al., 2009; Lisman and Jensen, 2013; Yamamoto et al., 2014). Vamp1 regulation may also be important in the cortical processing of sensory input, which relies on fast spiking PV^+ cells to distinguish preferred stimuli, recruit specific principal cell populations and modulate sensitivity to stimuli. (Hu et al., 2014; Isaacson and Scanziani, 2011; Tremblay et al., 2016; Xue et al., 2014). Dynamic changes in Vamp1 levels could alter the window of input integration in feedforward circuits, or change the population of excitatory neurons recruited in response to different stimuli.

Rbfox1 regulation of E/I balance and implications in neurologic disease

Mutation and/or dysregulation of Rbfox1 has been implicated in epilepsy and autism spectrum disorders (ASD). *Rbfox1*/RBFOX1 was identified as a candidate ASD susceptibility gene (Bhalla et al., 2004; Bill et al., 2013; Martin et al., 2007; Sebat et al., 2007; Voineagu et al., 2011), and changes in both Rbfox1-mediated gene expression (Lee et al., 2016) and alternative splicing (Parikshak et al., 2016; Voineagu et al., 2011; Weyn-Vanhentenryck et al., 2014) have been observed in ASD patient brains. Recent work found that cytoplasmic Rbfox1 targets, including Vamp1, showed significant overlap with genes involved in ASD (Lee et al., 2016). Mutations in RBFOX1 and RBFOX3 are also potential risk factors in a range of epileptic disorders (Lal et al., 2015; 2013a; 2013b). E/I balance and altered network oscillations are thought to be dysregulated in ASD (Gogolla et al., 2009; Hammer et al., 2015; Jurgensen and Castillo, 2015; Lee et al., 2015; Nakamura et al., 2015; Pizzarelli and Cherubini, 2011; Uhlhaas and Singer, 2006; van de Lagemaat et al., 2014; Yizhar et al., 2011) and epilepsy (Fritschy, 2008; Lee et al., 2015; Peñagarikano et al., 2011). In one study, using optogenetic tools to increase of the E/I ratio led to ASD-like impairments in social and cognitive function in mice and to changes in baseline gamma oscillations (Yizhar et al., 2011). Our finding that Vamp1 expression in inhibitory neurons rescues not only inhibitory but also excitatory synaptic transmission indicates that the reduced Vamp1 is a major component of the E/I imbalance seen in response to the Rbfox1 mutation. Changes in Rbfox1 function may thus underlie the changes in inhibitory signaling and E/I balance associated with these diseases (Marín, 2012).

Individual neuronal cell-types exhibit specific susceptibilities to Rbfox1 loss

Although the Rbfox proteins are co-expressed in many neuronal cell types, their functions are not redundant. The proteins are highly homologous and exhibit similar binding activities *in vivo* (Damianov et al., 2016; Weyn-Vanhentenryck et al., 2014) and similar splicing regulatory activities *in vitro* (Tang et al., 2009; Underwood et al., 2005). However, the different phenotypes of the *Rbfox1* and *Rbfox2* knockout mice have hinted at the particular susceptibility of neuronal subpopulations to the loss of individual Rbfox paralogs (see also Figures S3 and S4 F–M). While our RNA-seq data revealed targets affecting both excitatory and inhibitory synapses, the shift in E/I ratio towards increased excitation, and the similarity of the Vamp1 depletion phenotype to that of the *Rbfox1 Nes-cKO*, indicate a greater effect on inhibitory signaling. Indeed, we find that the transcripts down-regulated by Rbfox1 loss are enriched for genes whose expression correlates with the expression of inhibitory neuron markers, while transcripts that increase in the cKO were enriched for genes associated with excitatory neuron marker expression (Kang et al., 2011) (Figure S1B). Similar to our findings that Vamp1 is specific to inhibitory neurons and is strongly down regulated by Rbfox1 loss, this analysis emphasizes how RBPs can function in distinct ways in different cell types. Rather than a general Rbfox regulatory program common to all neurons, neuronal subtypes have their own programs of posttranscriptional regulation leading to cell type specific patterns of gene expression.

The regulation of inhibitory neuron-specific Vamp1 by Rbfox1 provides a paradigm for how other broadly expressed RBPs may perform crucial functions in defined neuronal populations. There are many families of RNA-binding proteins that are expressed across multiple neuronal populations, and the consequences of RBP loss have mostly been studied after pan-neuronal or germline deletion. Similarly, RNA-seq and CLIP-seq analyses of these RBPs have identified their targets in whole-brain or mixed tissue samples. Our results indicate that examination of these other RNA regulators in specific cell types (Hwang et al., 2017) should yield important new understanding of their functions.

STAR*METHODS

CONTACT FOR REAGENT AND RESOURCE SHARING

Further information and requests for reagents can be fulfilled by Lead Contact Douglas L. Black (DougB@microbio.ucla.edu).

EXPERIMENTAL MODEL AND SUBJECT DETAILS

Mouse models—All breeding and experimental procedures were conducted in accordance with the National Institutes of Health guidelines and approved by the Institutional Animal Care and Use Committee of the University of California, Los Angeles. Generation of and genotyping protocols for *Rbfox1*$^{fl/fl}$ [*Rbfox1*$^{tm1.1Dblk}$; JAX strain 014089] and *Nestin-Cre* [*Tg(Nes-cre)1Kln*; JAX strain 003771] mice have been previously described (Gehman et al., 2011; Tronche et al., 1999) and further information can be found at http://www.jax.org/. *Rbfox1*$^{fl/fl}$ mice were originally generated in the 129S2/Sv strain and backcrossed 10 generations to C57BL/6J (Gehman et al., 2011). Both *Rbfox1*$^{fl/fl}$ and *Nestin-Cre* mice were maintained on a C57BL/6J background and group housed under standard conditions.

Rbfox1$^{fl/fl}$ animals were crossed to *Nes-Cre*$^{+/-}$ to generate heterozygous *Rbfox1*$^{fl/+}$;*Nes-Cre*$^{+/-}$. Heterozygous animals were crossed to *Rbfox1*$^{fl/fl}$ to generate litters containing wildtype (*Rbfox1*$^{fl/fl}$; *Nes-Cre*$^{+/+}$) and cKO (*Rbfox*$^{fl/fl}$;*Nes-Cre*$^{+/-}$) animals.

For RNA-seq, qPCR and immunoblot experiments, male littermates were sacrificed between P60 and P70 by CO_2 overdose followed by cervical dislocation. For immunohistochemistry, P60–P70 male littermates were anesthetized with a mixture of 100mg/kg Ketamine and 10mg/kg Xylazine, followed by transcardial perfusion with ice-cold 1x PBS and 4% paraformal-dehyde in 1x PBS. For electrophysiology experiments, P60–P70 male littermates were deeply anesthetized with isoflurane and sacrificed by decapitation. Stereotaxic injections were performed on P60–P70 male littermates and are further described below.

Primary neuronal culture—Embryonic day 16–18 C57BL/6J pregnant dams (Charles River Laboratories) were sacrificed by CO_2 overdose followed by cervical dislocation. Embryos were decapitated with sharp scissors, and hippocampi from males and females were dissected out into ice-cold Hank's Balanced Salt Solution (HBSS, Ca^{2+}- and Mg^{2+}-free) and randomly pooled. Hippocampi were trypsinized in a 37°C water bath for 10 minutes and mechanically dissociated, and cells were plated at a density of ~790 cells/mm^2 (for RNA or protein isolation) or 395 cells/mm^2 (for immunocytochemistry) on tissue culture-treated plates or nitric-acid treated glass coverslips coated with 0.1mg/mL poly-DL-lysine (Sigma-Aldrich) in 0.1M boric acid, pH 8.5. Cells were initially plated in Neurobasal (Gibco) based Plating Media containing B27 (Gibco), Glutamax (Gibco), 25μM glutamate and 25μM B-mercaptoethanol and subsequently fed with Neurobasal based Feeding Media containing B27 and Glutamax every 3 days beginning at 3 days *in vitro* (DIV3). Primary cultures were maintained in a 37°C incubator supplemented with 5% CO_2.

Heterologous cell culture—293T (female) and 293FT (female) cells were grown in Dulbecco's Modification of Eagle's Medium (DMEM, Corning MT-10-017-CV) with L-glutamine and 4.5g/L glucose, supplemented with 10% fetal bovine serum and penicillin-streptomycin, and maintained in a 37°C incubator with 5% CO_2. For transfection, cells were plated on poly-ornithine coated plates, grown to 60–70% confluency and transfected with indicated plasmids using Lipofectamine 2000 (Invitrogen) for 6 hours. Live 293T cells were visualized on a Nikon TE2000-S inverted microscope and imaged using a SPOT RT-KE 7.4 slider CCD camera (Diagnostic instruments), or lysed in RI-PA buffer for protein isolation 48 hours post-transfection. 293FT cells transfected for AAV production were processed as described below. All cell lines tested negative for mycoplasma contamination, but have not been further authenticated.

METHOD DETAILS

Electrophysiology

Slice Preparation: Mice were deeply anesthetized with isoflurane and following decapitation the brain was rapidly removed and placed into ice-cold N-Methyl-D-Glucamine (NMDG)-based cutting solution containing (in mM): 135 NMDG, 10 D-glucose, 4 $MgCl_2$, 0.5 $CaCl_2$, 1 KCl, 1.2 KH_2PO_4, and 26 HEPES (pH = 7.3–7.4, 290–300 mOsm/L), bubbled with 100% O_2. Coronal slices (320 μm) were prepared using a Campden 7000SMZ-2

Vibratome and then maintained in an interface-slice type chamber continuously perfused (2–3 mL/min) with a warm (30°C), oxygenated (95% O_2/5% CO_2) artificial cerebrospinal fluid (ACSF) containing (in mM): 124 NaCl, 2.4 KCl, 25 $NaHCO_3$, 1 NaH_2PO_4, 2 $CaCl_2$, 1.2 $MgSO_4$, and 10 glucose (pH 7.4, 290–300 mOsm). Slices were allowed to recover for at least 1 hour prior to recordings. All experimental techniques were approved by the Institutional Animal Care and Use Committee at the University of California, Los Angeles.

Patch-clamp recordings in brain slices and cultured neurons: Slices were transferred to a submerged-slice recording chamber continuously perfused (3 mL/min) with ACSF and whole-cell voltage-clamp techniques were used to record both evoked and miniature EPSCs and IPSCs. CA1 pyramidal cells and dentate gyrus granule cells were visualized using an IR-DIC upright microscope (Zeiss Examiner D1) and whole-cell recordings were performed using borosilicate patch electrodes (4–6 MΩ), containing (in mM): 120 $CsMeSO_4$, 10 CsCl, 5 TEA-Cl, 1.5 $MgCl_2$, 10 HEPES, 0.1 EGTA, 2 Na-ATP, 0.5 Na-GTP, and 5 QX-314, pH 7.25–7.30 with CsOH, 275–285 mOsm. Recordings were obtained using a MultiClamp 700B amplifier with Digidata 1440A and pClamp 10 (Molecular Devices). Series resistance and whole-cell capacitance were automatically compensated and recordings were discontinued if series resistance increased by >20%. A bipolar, tungsten wire stimulating electrode placed in stratum radiatum proximal to the CA3 region was used to activate Schaffer collateral/commissural fibers and elicit EPSCs and IPSCs in CA1 pyramidal cells (stimulation rate = 0.05 Hz). In these experiments, we isolated the excitatory and inhibitory components of the evoked responses by recording synaptic currents at holding potentials (V_{hold}) of −68 and +10 mV, respectively. Bath application of 20 μM CNQX and 50 μM APV blocked synaptic currents at V_{hold} = −68 mV while application of 100 μM picrotoxin blocked synaptic currents at V_{hold} = +10 mV, confirming that EPSCs and IPSCs are isolated at these membrane potentials (data not shown). The intensity of presynaptic fiber stimulation was adjusted to elicit EPSCs with a peak amplitude of 100–300 pA at V_{hold} = −68 mV, and with the same stimulating intensity to record IPSCs at V_{hold} = +10 mV. Miniature EPSCs and IPSCs were recorded in the presence of 1 μM TTX. In experiments recording EPSCs and IPSCs in cultured neurons, cells were bathed in an external solution containing (in mM): 140 NaCl, 3 KCl, 2 $CaCl_2$, 1 $MgCl_2$, 10 D-glucose, 26 HEPES, and 1 μM TTX (pH = 7.4, 290–300 mOsm/L).

Data analysis and chemicals: Evoked currents were analyzed in Clampfit 10, and amplitude was measured as the peak of currents. Miniature E/IPSCs were detected and analyzed with custom-written LabView-based software. All results are presented as mean ± s.e.m. Statistical significance was determined using unpaired *t* tests. Picrotoxin and TTX were purchased from Tocris Biosciences. All other chemicals were from Sigma-Aldrich.

Stereotaxic injections—Adult (P60–P70) male littermates were anesthetized with 5% isoflurane and 33% N_2O mixed with O_2. Hair on the head was shaved following anesthesia, and animals were given 0.1mg/kg buprenorphine via intraperitoneal injection. Animals were fitted to a stereotaxic frame with blunt ear bars and provided with the same anesthesia mixture for the duration of the surgery. Skin on the head was sterilized with 70% ethanol and 10% povidone iodine, and an incision in the skin was made followed by craniotomies 2–

3mm in diameter above the left and right hippocampi at −2.0mm posterior to Bregma and +/−1.5mm lateral to the midline. A glass micropipette driven by a syringe pump was used to deliver 3.9 E+12 genome copies (~1μl) of AAV2/9 mDlx-tRFP or AAV2/9 mDlx-tRFP-p2A-Vamp1r to CA1 at a depth of −1.6mm relative to the pial surface, at a rate of 0.2uL/minute. The pipette was left in place for 6 minutes after injection and withdrawn slowly over a 5-minute interval. The surgical incision was closed with external nylon sutures. Animals recovered in their home cages and were given intraperitoneal 0.1mg/kg bu-prenorphine twice daily for 3 days afterward. Animals were sacrificed three weeks post-injection for electrophysiology or transcardially perfused for immunohistochemistry.

RNA sequencing—Three pairs of P60–P70 *Rbfox1 Nes-cKO* and wildtype male littermates from different litters were sacrificed and hippocampi were dissected out in ice-cold HBSS. Hippocampi were lysed in Trizol (Invitrogen) using a Tissue Tearor and RNA was extracted according to the manufacturer's instructions. 1ug of total RNA was used for polyA selection and library construction using the Tru-Seq mRNA Stranded Library Kit (Illumina). Isolated PolyA-plus RNA was converted to cDNA and subjected to 50 nt paired-end sequencing using the standard Illumina platform on a Hi-Seq 2000.

Quantitative PCR

Relative gene expression: Trizol-extracted RNA was subjected to DNAse treatment (DNAseI, Roche) and purified by acidic phenol-chloroform extraction. 1ug of total RNA and oligo$(dT)_{18}$ primers were used for reverse transcription by Superscript III (Invitrogen), and equal volumes of cDNA across samples were used for qPCR using the SensiFAST SYBR Lo-ROX qPCR mix in a QuantStudio6 (Applied Biosystems). All relative fold change quantifications were normalized to expression of the housekeeping gene, Hprt.

Absolute quantitation: DNAse-treated RNA was extracted and reverse transcribed as described above. For spliced and unspliced Vamp1 transcripts, cDNA from brain samples was quantified against a standard curve of 10-fold dilutions of spliced or unspliced products ranging from 10^3–10^8 nM. For quantitation of AAV titer, an aliquot of the virus was treated with DNAse, followed by DNAse inhibition and Proteinase K treatment to release the viral genome. Viral genomes were quantified against a standard curve of the cognate AAV genome plasmid ranging from 5×10^1–5×10^8 copies/μl to obtain a titer of genome copies (GC) per mL.

Taqman assay: DNAse-treated RNA was extracted as described above, and 10ng of total RNA was used for reverse transcription (RT) using the Multiscribe Reverse Transcriptase (ThermoFisher) and primers specific to the mature *mmu-miR-9* or, as a control, *U6* snRNA. The RT product was then amplified using fluorescent Taqman-MGB probes specific for *miR-9* or *U6*. Relative fold changes in *miR-9* levels were normalized to *U6*.

DNA constructs and adeno-associated viruses

Luciferase reporters: pGL3-control (Promega) was used to insert the full length (FL) or a portion (3′F) of the *Vamp1* 3′UTR following the *Luciferase* gene using the NdeI and FseI restriction sites. Mutations of Rbfox binding sites in the 3′UTR from (U)GCAUG to

(U)G*ACGU* and of the *miR9* seed site from CCAAAG to *GGUU*AG were created using site-directed mutagenesis and subcloned into pGL3-control.

RNAi constructs: The pAAV-U6-shLuc-CMV-GFP plasmid was used as a backbone to insert a hairpin targeting the *Vamp1* coding sequence (5′-GAGCAGTGCTGCCAAGCTAAA-3′) using the BamHI and EcoRI restriction sites.

Vamp expression constructs: The *Vamp1* coding sequence (NM_009496.3) was generated as a gBlock (IDT) along with *p2A-tRFP* and cloned into pcDNA3.1(+) using BamHI and EcoRI, or into pAAV-hSyn-Cre-WPRE-hGH (University of Pennsylvania Vector Core Facility #PL-C-PV1969) using AgeI and EcoRI. The Vamp2 construct in pcDNA3.1(+) was similarly created using the *Vamp2* coding sequence (NM_009497.3). A tRFP-p2A-Vamp1r RNAi-resistant gBlock containing silent mutations within the shRNA targeting region was cloned into pcDNA3.1(+) and pAAV-hSyn-Cre-WPRE-hGH using the same restriction sites as above to create rescue constructs. The pAAV-mDlx-GFP-Fishell-1 plasmid (Addgene #83900) was used as a backbone to insert either tRFP or tRFP-p2A-Vamp1r using the SpeI and AscI restriction sites to create pAAV-mDlx-tRFP and pAAV-mDlx-tRFP-p2A-Vamp1r.

Tough Decoy constructs: Tough decoy sequences were designed according to ((Haraguchi et al., 2009); Figure 2). The mature *miR-9* targeting sequence is 5′-CTCATACAGCTA*ATCT*GATAACCAAAGA-3′, and the control sequence is 5′-CGCGACTATACG*ATCT*CGCAATATGGT-3′, where the *ATCT* is not complementary to the mature *miR* sequence and produces a bulge. The control TuD sequence was obtained from a negative control sequence for mouse as validated by IDT (IDT© miRNA Inhibitors). Synthetic oligos of TuD stem loops containing the mature *miR-9* or control sequence were annealed and inserted into pAAV-U6-shLuc-CMV-eGFP-SV40 (University of Pennsylvania Vector Core Facility # PL-C-PV1867) using the BamHI and EcoRI sites. CMV-eGFP was replaced with hSyn-tRFP using XbaI and NotI.

Adeno-associated viruses: All AAV were packaged with capsid serotype 9. AAV2/9 mDlx-tRFP, mDlx-tRFP-p2A-Vamp1r, U6-TuDctrl-hSyn-tRFP and U6-TuDmiR9-hSyn-tRFP were produced by co-transfection of the AAV2 genomic plasmid, pHelper and an AAV9 envelope plasmid into 293FT cells. Viral particles were obtained from the cell pellet and media at 3 and 5 days posttransfection by polyethyleneglycol (PEG) precipitation, purified using an ioxodianol gradient and concentrated using an Amicon centrifugal filter with a 100kDa membrane. Viral titer was determined by qPCR using a standard curve of the genome plasmid. AAV2/9 hSyn-Rbfox1-cytoplasmic was previously described [hSyn.Flag-Rbfox1_c_siMt] (Lee et al., 2016), and U6-Vamp1sh#5-CMV-GFP and U6-shLuc-CMV-GFP viruses were generated at the University of Pennsylvania Vector Core Facility. AAV2/9 hSyn-eGFP and AAV2/9 hSyn-Cre-eGFP viruses were also purchased from the University of Pennsylvania Vector Core Facility.

Vamp1 knockdown—Wildtype primary neurons were isolated from E16–E18 embryos and plated at a density of ~790 cells/mm^2 on poly-DL-lysine coated nitric-acid treated coverslips. Cells were transduced at DIV8 with AAV2/9 U6-Vamp1sh#5-CMV-GFP or AAV2/9 U6-shLuc-CMV-GFP. Vamp1 knockdown cells were additionally transduced with

either AAV2/9 mDlx-tRFP or AAV2/9 mDlx-tRFP-p2A-Vamp1r (RNAi-resistant) at the same time. mIPSCs and mEPSCs were recorded at DIV15-17, when Vamp1 expression normally peaks (data not shown).

Luciferase Assays—Primary hippocampal neurons were isolated from E16–18 *Rbfox1*$^{fl/fl}$ embryos and plated at a density of ~790 cells/mm^2 on poly-DL-lysine coated 96-well plates. Cells were transduced at DIV3 with AAV2/9 *hSyn*-eGFP or AAV2/9 *hSyn*-Cre-eGFP and co-transfected at DIV5 with pRL-TK Renilla and pGL3 Luciferase reporters using Lipofectamine 2000. For experiments using Tough Decoys, cells were transduced again at DIV7 with AAV2/9 U6-TuDctrl-hSyn-tRFP or AAV2/9 U6-TuDmiR9-hSyn-tRFP. Cells were collected at DIV14 for luciferase assay using the Dual-Glo Luciferase Kit (Promega) as directed and analysed using a Synergy2 Multi-Mode Reader (Biotek).

Immunoblotting—P60–P70 mice were sacrificed and brain tissue was dissected out in ice-cold HBSS. Tissue was lysed in RIPA buffer with protease and phosphatase inhibitors (Roche) and benzonase using a Tissue Tearor. Lysates were cleared and boiled in SDS loading buffer, separated on 10% or 12% Tris-glycine gels and transferred to 0.45μm PVDF membranes (GE Amersham). Membranes were imaged on a Typhoon Variable Mode Imager 9410 (GE Amersham Bioscience) and quantified using ImageQuantTL software version 8.1. The following primary antibodies were used: ms α-Rbfox1 clone 1D10 (EMD Millipore), 1:2000; rb α-Vamp1, 1:1000 (Synaptic Systems); gp α-Vamp2, 1:1000 (Synaptic Systems); ms α-GAPDH clone 6C5, 1:4000 (Ambion). Cy3- or Cy5-conjugated secondary antibodies against –ms, -rb or –gp were used at 1:2500 (GE Healthcare).

Immunocytochemistry and immunohistochemistry

Immunocytochemistry: Primary hippocampal neurons grown on nitric-acid treated coverslips were fixed at DIV18 in 4% paraformaldehyde/PBS. Fixed cells were permeablized with 0.1% Triton/PBS and blocked with 10% goat serum/PBS. Primary antibodies were incubated overnight at 4C, followed by 3 washes and secondary antibody incubation for 2hrs at room temperature. Antibodies were diluted in 3% BSA with 0.02% sodium azide in PBS. Coverslips were mounted using ProLong Gold (Invitrogen) and imaged on Zeiss LSM 510 Meta and LSM 780 confocal microscopes using 40x or 63x oil objectives as indicated in each figure legend.

Immunohistochemistry: Adult *Rbfox1 Nes-cKO* and wildtype littermates were transcardially perfused with ice-cold PBS followed by ice-cold 4% paraformaldehyde/PBS. Brains were further fixed in 4% paraformaldehyde/PBS overnight at 4C, then cryoprotected in 30% sucrose and embedded in OCT compound (Tissue-Tek). 40μm frozen sections were cut in coronal orientation using a Leica Microm HM505E cryostat onto SuperFrost Plus (VWR) glass slides. Sections were rehydrated in PBS, permeablized with 0.5% Triton/PBS and blocked with 10% goat serum in 0.5% Triton/PBS for 1 hour at room temperature. Sections were incubated with primary antibodies overnight at 4C, followed by 3 washes and secondary antibody incubation for 2hrs at room temperature. Antibodies were diluted in 3% BSA with 0.02% sodium azide in PBS. Sections were mounted in ProLong Gold and imaged

using 10x, 20x air or 40x, 63x oil objectives as indicated in each figure legend on Zeiss LSM 510 Meta and LSM 780 confocal microscopes.

The following antibodies were used: ms α-Rbfox1 clone 1D10 (EMD Millipore), 1:2000; rb α-Vamp1, 1:1000 (Synaptic Systems); gp α-Vamp2, 1:1000 (Synaptic Systems); ms α-Gad67 clone 1G10.2, 1:1000 (EMD-Millipore); rb α-Gephyrin, 1:1000 (Synaptic Systems); ch α-Map2, 1:2000 (Abcam); ms α-PSD-95, 1:1000 (Antibodies Incorporated); gp α-Synaptophysin, 1:1000 (Synaptic Systems); ms α-znp-1 (Synaptotagmin2), 1:1000 (ZIRC); gp α-Parvalbumin, 1:1000 (Synaptic Systems). Alexa Fluor 488-, 568- or 647-conjugated goat α –mouse, -rabbit, -chicken or –guinea pig secondary antibodies (Thermo Fisher) were used at a dilution of 1:1000 for 488 and 568, and 1:500 for 647.

QUANTIFICATION AND STATISTICAL ANALYSES

Quantitative data are presented as mean ± s.e.m. All experiments were independently repeated at least three times. See figure legends for statistical details and significance of each experiment.

Quantification of pre-synaptic puncta—All quantification was done by hand in ImageJ (Schneider et al., 2012). Cultured neurons used for quantification were imaged at 63x magnification. For VAMP1 co-localization with excitatory or inhibitory markers (Figure 3A,B), puncta were counted within 100μm^2 areas in a total of 15 images from 1 culture (biological replicate). For co-localization of excitatory or inhibitory pre- and post-synaptic puncta (Figure S5B, C), puncta were counted along 3–4 50μm dendritic sections per image, from 5–6 images per culture, in 3–4 cultures (biological replicates).

Tissue sections used for quantification were imaged at 40x magnification. For VAMP1 puncta co-localization with GAD67 or SYT2 in CA1 (Figure 3C–F), puncta were counted within at least (3) 50μm^2 areas/image, in a total of 3 images per animal (n=3 animals). For VAMP1 puncta co-localization with GAD67 or SYT2 in DG (Figure S3B–E), puncta were counted within at least 2 (DG hilus) or 3 (DG sp and ip) 50μm^2 fields/image, in a total of 1 (DG hilus) or 2 (DG sp and ip) images per animal (n=3 animals).

RNA-seq analysis—An average of 48 million reads were generated per replicate sample. Reads were aligned to the mouse genome (mm9) using TopHat version 2.0.10 (Trapnell et al., 2012) with an average mapping rate of 90%. Spliced isoform analysis was done using SpliceTrap version 0.92 (Table S1) (Wu et al., 2011). Events with changes in percent spliced in |delta PSI| > 10% and read coverage exon 1> 50 and exon 3 > 50 in both samples were considered significant. Overall expression levels were detected using the Cufflinks package version 2.2.1 (Table S2) (Trapnell et al., 2012). For differential gene expression, $q<0.05$ and log2 fold-change ≥1.2 was used to define significant changes.

Enrichment analysis in specific cell subtypes—Logistic regression was used to assess enrichment of Rbfox1-regulated transcripts in inhibitory and excitatory cell subtypes (Figure S1B). “Enriched genes” are those with an FDR adjusted $p<0.05$ for the respective cell type. Cell-specific gene lists encompass the top 100 genes correlated to canonical

markers of specific subtypes of inhibitory and excitatory cell types in a spatiotemporal atlas of human brain expression (Kang et al., 2011).

DATA AND SOFTWARE AVAILABILITY

The RNA-seq data reported in this paper has been deposited in the Gene Expression Omnibus under ID code GSE96722.

Supplementary Material

Refer to Web version on PubMed Central for supplementary material.

Acknowledgments

We thank G. Fishell (HMS), X. Jaglin and B. Wamsley (NYU) for the *mDlx* AAV plasmid, their thoughtful feedback and manuscript coordination; B. Khakh, J.C. Octeau (UCLA) and R. Srinivisan (Texas A&M) for invaluable help with stereotaxic injections; X.W. Yang and C. Park (UCLA) for the AAV production protocol and plasmids; D.H. Geschwind for help with informatics analyses; members of the D.L.B, T.J.O. and K.C.M. labs for helpful discussions; and the sequencing and imaging cores at the Broad Stem Cell Research Center at UCLA. This work was supported by NIH Grants T32 GM007185 and F31 NS093923 to C.K.V., R01 GM114463 to D.L.B., R01 MH060919 to T.J.O., R21 MH101684 to K.C.M., and a NARSAD Young Investigator Award to J.A.L.

References

Atallah BV, Scanziani M. Instantaneous modulation of gamma oscillation frequency by balancing excitation with inhibition. Neuron. 2009; 62:566–577. [PubMed: 19477157]

Bak RO, Hollensen AK, Primo MN, Sørensen CD, Mikkelsen JG. Potent microRNA suppression by RNA Pol II-transcribed “Tough Decoy” inhibitors. Rna. 2013; 19:280–293. [PubMed: 23249752]

Bartos M, Vida I, Jonas P. Synaptic mechanisms of synchronized gamma oscillations in inhibitory interneuron networks. Nat Rev Neurosci. 2007; 8:45–56. [PubMed: 17180162]

Bhalla K, Phillips HA, Crawford J, McKenzie OLD, Mulley JC, Eyre H, Gardner AE, Kremmidiotis G, Callen DF. The de novo chromosome 16 translocations of two patients with abnormal phenotypes (mental retardation and epilepsy) disrupt the A2BP1 gene. J Hum Genet. 2004; 49:308–311. [PubMed: 15148587]

Bill BR, Lowe JK, Dybuncio CT, Fogel BL. Orchestration of neurodevelop-mental programs by RBFOX1: implications for autism spectrum disorder. Int Rev Neurobiol. 2013; 113:251–267. [PubMed: 24290388]

Buzsáki G, Wang X-J. Mechanisms of gamma oscillations. Annu Rev Neurosci. 2012; 35:203–225. [PubMed: 22443509]

Cardin JA, Carlén M, Meletis K, Knoblich U, Zhang F, Deisseroth K, Tsai LH, Moore CI. Driving fast-spiking cells induces gamma rhythm and controls sensory responses. Nature. 2009; 459:663–667. [PubMed: 19396156]

Carreira-Rosario A, Bhargava V, Hillebrand J, Kollipara RK, Ramaswami M, Buszczak M. Repression of Pumilio Protein Expression by Rbfox1 Promotes Germ Cell Differentiation. Dev Cell. 2016; 36:562–571. [PubMed: 26954550]

Chabot B, Shkreta L. Defective control of pre-messenger RNA splicing in human disease. The Journal of Cell Biology. 2016; 212:13–27. [PubMed: 26728853]

Colgin LL, Denninger T, Fyhn M, Hafting T, Bonnevie T, Jensen O, Moser MB, Moser EI. Frequency of gamma oscillations routes flow of information in the hippocampus. Nature. 2009; 462:353–357. [PubMed: 19924214]

Conboy JG. Developmental regulation of RNA processing by Rbfox proteins. Wiley Interdiscip Rev RNA. 2017; 8:e1398.

Coolen M, Katz S, Bally-Cuif L. miR-9: a versatile regulator of neurogenesis. Front Cell Neurosci. 2013; 7:220. [PubMed: 24312010]

Dajas-Bailador F, Bonev B, Garcez P, Stanley P, Guillemot F, Papalopulu N. microRNA-9 regulates axon extension and branching by targeting Map1b in mouse cortical neurons. Nat Neurosci. 2012; 15:697–699.

Damianov A, Ying Y, Lin CH, Lee JA, Tran D, Vashisht AA, Bahrami-Samani E, Xing Y, Martin KC, Wohlschlegel JA, et al. Rbfox Proteins Regulate Splicing as Part of a Large Multiprotein Complex LASR. Cell. 2016; 165:606–619. [PubMed: 27104978]

Deák F, Shin OH, Kavalali ET, Südhof TC. Structural determinants of synaptobrevin 2 function in synaptic vesicle fusion. Journal of Neuroscience. 2006; 26:6668–6676. [PubMed: 16793874]

Delaloy C, Liu L, Lee JA, Su H, Shen F, Yang GY, Young WL, Ivey KN, Gao FB. MicroRNA-9 coordinates proliferation and migration of human embryonic stem cell-derived neural progenitors. Cell Stem Cell. 2010; 6:323–335. [PubMed: 20362537]

Dimidschstein J, Chen Q, Tremblay R, Rogers SL, Saldi GA, Guo L, Xu Q, Liu R, Lu C, Chu J, et al. A viral strategy for targeting and manipulating interneurons across vertebrate species. Nat Neurosci. 2016; 19:1743–1749. [PubMed: 27798629]

Ferecskó AS, Jiruska P, Foss L, Powell AD, Chang WC, Sik A, Jefferys JGR. Structural and functional substrates of tetanus toxin in an animal model of temporal lobe epilepsy. Brain Struct Funct. 2015; 220:1013–1029. [PubMed: 24442865]

Friedman RC, Farh KK-H, Burge CB, Bartel DP. Most mammalian mRNAs are conserved targets of microRNAs. Genome Res. 2009; 19:92–105. [PubMed: 18955434]

Fritschy JM. Epilepsy, E/I Balance and GABA(A) Receptor Plasticity. Front Mol Neurosci. 2008; 1:5. [PubMed: 18946538]

Fu AKY, Hung KW, Fu WY, Shen C, Chen Y, Xia J, Lai KO, Ip NY. APC(Cdh1) mediates EphA4-dependent downregulation of AMPA receptors in homeostatic plasticity. Nat Neurosci. 2011; 14:181–189. [PubMed: 21186356]

Gehman LT, Stoilov P, Maguire J, Damianov A, Lin CH, Shiue L, Ares M, Mody I, Black DL. The splicing regulator Rbfox1 (A2BP1) controls neuronal excitation in the mammalian brain. Nature Publishing Group. 2011; 43:706–711.

Giusti SA, Vogl AM, Brockmann MM, Vercelli CA, Rein ML, Trümbach D, Wurst W, Cazalla D, Stein V, Deussing JM, et al. MicroRNA-9 controls dendritic development by targeting REST. Elife. 2014; 3:14.

Gogolla N, Leblanc JJ, Quast KB, Südhof TC, Fagiolini M, Hensch TK. Common circuit defect of excitatory-inhibitory balance in mouse models of autism. J Neurodev Disord. 2009; 1:172–181. [PubMed: 20664807]

Grimson A, Farh KKH, Johnston WK, Garrett-Engele P, Lim LP, Bartel DP. MicroRNA targeting specificity in mammals: determinants beyond seed pairing. Mol Cell. 2007; 27:91–105. [PubMed: 17612493]

Hammer M, Krueger-Burg D, Tuffy LP, Cooper BH, Taschenberger H, Goswami SP, Ehrenreich H, Jonas P, Varoqueaux F, Rhee JS, et al. Perturbed Hippocampal Synaptic Inhibition and γ-Oscillations in a Neuroligin-4 Knockout Mouse Model of Autism. Cell Rep. 2015; 13:516–523. [PubMed: 26456829]

Haraguchi T, Ozaki Y, Iba H. Vectors expressing efficient RNA decoys achieve the long-term suppression of specific microRNA activity in mammalian cells. Nucleic Acids Research. 2009; 37:e43–e43. [PubMed: 19223327]

Hu H, Gan J, Jonas P. Interneurons. Fast-spiking, parvalbumin^{+} GABAergic interneurons: from cellular design to microcircuit function. Science. 2014; 345:1255263–1255263. [PubMed: 25082707]

Hwang HW, Saito Y, Park CY, Blachère NE, Tajima Y, Fak JJ, Zucker-Scharff I, Darnell RB. cTag-PAPERCLIP Reveals Alternative Polyadenylation Promotes Cell-Type Specific Protein Diversity and Shifts Araf Isoforms with Microglia Activation. Neuron. 2017; 95:1334–1349. e1335. [PubMed: 28910620]

Isaacson JS, Scanziani M. How inhibition shapes cortical activity. Neuron. 2011; 72:231–243. [PubMed: 22017986]

Jin Y, Suzuki H, Maegawa S, Endo H, Sugano S, Hashimoto K, Yasuda K, Inoue K. A vertebrate RNA-binding protein Fox-1 regulates tissue-specific splicing via the pentanucleotide GCAUG. Embo J. 2003; 22:905–912. [PubMed: 12574126]

Jonas P, Bischofberger J, Fricker D, Miles R. Interneuron Diversity series: Fast in, fast out--temporal and spatial signal processing in hippocampal interneurons. Trends in Neurosciences. 2004; 27:30–40. [PubMed: 14698608]

Jurgensen S, Castillo PE. Selective Dysregulation of Hippocampal Inhibition in the Mouse Lacking Autism Candidate Gene CNTNAP2. Journal of Neuroscience. 2015; 35:14681–14687. [PubMed: 26511255]

Kang HJ, Kawasawa YI, Cheng F, Zhu Y, Xu X, Li M, Sousa AMM, Pletikos M, Meyer KA, Sedmak G, et al. Spatiotemporal transcriptome of the human brain. Nature. 2011; 478:483–489. [PubMed: 22031440]

Kuroyanagi H. Fox-1 family of RNA-binding proteins. Cell Mol Life Sci. 2009; 66:3895–3907. [PubMed: 19688295]

Lal D, Pernhorst K, Klein KM, Reif P, Tozzi R, Toliat MR, Winterer G, Neubauer B, Nürnberg P, Rosenow F, et al. Extending the phenotypic spectrum of RBFOX1 deletions: Sporadic focal epilepsy. Epilepsia. 2015; 56 n/a–n/a.

Lal D, Reinthaler EM, Altmüller J, Toliat MR, Thiele H, Nürnberg P, Lerche H, Hahn A, Møller RS, Muhle H, et al. RBFOX1 and RBFOX3 mutations in rolandic epilepsy. PLoS ONE. 2013a; 8:e73323. [PubMed: 24039908]

Lal D, Trucks H, Møller RS, Hjalgrim H, Koeleman BPC, de Kovel CGF, Visscher F, Weber YG, Lerche H, Becker F, et al. Rare exonic deletions of the RBFOX1 gene increase risk of idiopathic generalized epilepsy. Epilepsia. 2013b; 54:265–271. [PubMed: 23350840]

Lee JA, Tang ZZ, Black DL. An inducible change in Fox-1/A2BP1 splicing modulates the alternative splicing of downstream neuronal target exons. Genes Dev. 2009; 23:2284–2293. [PubMed: 19762510]

Lee JA, Damianov A, Lin CH, Fontes M, Parikshak NN, Anderson ES, Geschwind DH, Black DL, Martin KC. Cytoplasmic Rbfox1 Regulates the Expression of Synaptic and Autism-Related Genes. Neuron. 2016; 89:113–128. [PubMed: 26687839]

Lee J, Chung C, Ha S, Lee D, Kim DY, Kim H, Kim E. Shank3-mutant mice lacking exon 9 show altered excitation/inhibition balance, enhanced rearing, and spatial memory deficit. Front Cell Neurosci. 2015; 9:94. [PubMed: 25852484]

Lewis BP, Burge CB, Bartel DP. Conserved seed pairing, often flanked by adenosines, indicates that thousands of human genes are microRNA targets. Cell. 2005; 120:15–20. [PubMed: 15652477]

Licatalosi DD, Darnell RB. Splicing regulation in neurologic disease. Neuron. 2006; 52:93–101. [PubMed: 17015229]

Lisman JE, Jensen O. The θ-γ neural code. Neuron. 2013; 77:1002–1016. [PubMed: 23522038]

Liu DZ, Ander BP, Tian Y, Stamova B, Jickling GC, Davis RR, Sharp FR. Integrated analysis of mRNA and microRNA expression in mature neurons, neural progenitor cells and neuroblastoma cells. Gene. 2012; 495:120–127. [PubMed: 22244746]

Liu Y, Sugiura Y, Lin W. The role of synaptobrevin1/VAMP1 in Ca2+-triggered neurotransmitter release at the mouse neuromuscular junction. The Journal of Physiology. 2011; 589:1603–1618. [PubMed: 21282288]

Malmevik J, Petri R, Knauff P, Brattås PL, Åkerblom M, Jakobsson J. Distinct cognitive effects and underlying transcriptome changes upon inhibition of individual miR-NAs in hippocampal neurons. Sci Rep. 2016; 6:19879. [PubMed: 26813637]

Marín O. Interneuron dysfunction in psychiatric disorders. Nat Rev Neurosci. 2012; 13:107–120. [PubMed: 22251963]

Martin CL, Duvall JA, Ilkin Y, Simon JS, Arreaza MG, Wilkes K, Alvarez-Retuerto A, Whichello A, Powell CM, Rao K, et al. Cytogenetic and molecular characterization of A2BP1/FOX1 as a candidate gene for autism. Am J Med Genet B Neuropsychiatr Genet. 2007; 144B:869–876. [PubMed: 17503474]

Nakahata S, Kawamoto S. Tissue-dependent isoforms of mammalian Fox-1 homologs are associated with tissue-specific splicing activities. Nucleic Acids Research. 2005; 33:2078–2089. [PubMed: 15824060]

Nakamura T, Matsumoto J, Takamura Y, Ishii Y, Sasahara M, Ono T, Nishijo H. Relationships among parvalbumin-immunoreactive neuron density, phase-locked gamma oscillations, and autistic/schizophrenic symptoms in PDGFR-β knock-out and control mice. PLoS ONE. 2015; 10:e0119258. [PubMed: 25803852]

Nystuen AM, Schwendinger JK, Sachs AJ, Yang AW, Haider NB. A null mutation in VAMP1/synaptobrevin is associated with neurological defects and prewean mortality in the lethal-wasting mouse mutant. Neurogenetics. 2007; 8:1–10. [PubMed: 17102983]

Parikshak NN, Swarup V, Belgard TG, Irimia M, Ramaswami G, Gandal MJ, Hartl C, Leppa V, de Ubieta LLT, Huang J, et al. Genome-wide changes in lncRNA, splicing, and regional gene expression patterns in autism. Nature. 2016; 540:423–427. [PubMed: 27919067]

Peñagarikano O, Abrahams BS, Herman EI, Winden KD, Gdalyahu A, Dong H, Sonnenblick LI, Gruver R, Almajano J, Bragin A, et al. Absence of CNTNAP2 leads to epilepsy, neuronal migration abnormalities, and core autism-related deficits. Cell. 2011; 147:235–246. [PubMed: 21962519]

Pizzarelli R, Cherubini E. Alterations of GABAergic signaling in autism spectrum disorders. Neural Plast. 2011; 2011:297153–12. [PubMed: 21766041]

Ponthier JL, Schluepen C, Chen W, Lersch RA, Gee SL, Hou VC, Lo AJ, Short SA, Chasis JA, Winkelmann JC, et al. Fox-2 splicing factor binds to a conserved intron motif to promote inclusion of protein 4.1R alternative exon 16. J Biol Chem. 2006; 281:12468–12474. [PubMed: 16537540]

Pouille F, Scanziani M. Enforcement of temporal fidelity in pyramidal cells by somatic feed-forward inhibition. Science. 2001; 293:1159–1163. [PubMed: 11498596]

Poulos MG, Batra R, Charizanis K, Swanson MS. Developments in RNA splicing and disease. Cold Spring Harbor Perspectives in Biology. 2011; 3:a000778–a000778. [PubMed: 21084389]

Qiu Z, Sylwestrak EL, Lieberman DN, Zhang Y, Liu XY, Ghosh A. The Rett syndrome protein MeCP2 regulates synaptic scaling. Journal of Neuroscience. 2012; 32:989–994. [PubMed: 22262897]

Schneider CA, Rasband WS, Eliceiri KW. NIH Image to ImageJ: 25 years of image analysis. Nat Meth. 2012; 9:671–675.

Schoch S, Deák F, Königstorfer A, Mozhayeva M, Sara Y, Südhof TC, Kavalali ET. SNARE function analyzed in synaptobrevin/VAMP knockout mice. Science. 2001; 294:1117–1122. [PubMed: 11691998]

Sebat J, Lakshmi B, Malhotra D, Troge J, Lese-Martin C, Walsh T, Yamrom B, Yoon S, Krasnitz A, Kendall J, et al. Strong association of de novo copy number mutations with autism. Science. 2007; 316:445–449. [PubMed: 17363630]

Shi Z, Luo G, Fu L, Fang Z, Wang X, Li X. miR-9 and miR-140-5p target FoxP2 and are regulated as a function of the social context of singing behavior in zebra finches. Journal of Neuroscience. 2013; 33:16510–16521. [PubMed: 24133256]

Sim SE, Lim CS, Kim JI, Seo D, Chun H, Yu NK, Lee J, Kang SJ, Ko HG, Choi JH, et al. The Brain-Enriched MicroRNA miR-9-3p Regulates Synaptic Plasticity and Memory. Journal of Neuroscience. 2016; 36:8641–8652. [PubMed: 27535911]

Sommeijer JP, Levelt CN. Synaptotagmin-2 is a reliable marker for parvalbu-min positive inhibitory boutons in the mouse visual cortex. PLoS ONE. 2012; 7:e35323. [PubMed: 22539967]

Srikantan S, Gorospe M. HuR function in disease. Front Biosci (Landmark Ed). 2012; 17:189–205. [PubMed: 22201738]

Sun AX, Crabtree GR, Yoo AS. MicroRNAs: regulators of neuronal fate. Current Opinion in Cell Biology. 2013; 25:215–221. [PubMed: 23374323]

Tang ZZ, Zheng S, Nikolic J, Black DL. Developmental Control of CaV1.2 L-Type Calcium Channel Splicing by Fox Proteins. Molecular and Cellular Biology. 2009; 29:4757–4765. [PubMed: 19564422]

Trapnell C, Roberts A, Goff L, Pertea G, Kim D, Kelley DR, Pimentel H, Salzberg SL, Rinn JL, Pachter L. Differential gene and transcript expression analysis of RNA-seq experiments with TopHat and Cufflinks. Nat Protoc. 2012; 7:562–578. [PubMed: 22383036]

Tremblay R, Lee S, Rudy B. GABAergic Interneurons in the Neocortex: From Cellular Properties to Circuits. Neuron. 2016; 91:260–292. [PubMed: 27477017]

Tronche F, Kellendonk C, Kretz O, Gass P, Anlag K, Orban PC, Bock R, Klein R, Schütz G. Disruption of the glucocorticoid receptor gene in the nervous system results in reduced anxiety. Nat Genet. 1999; 23:99–103. [PubMed: 10471508]

Turrigiano G. Too many cooks? Intrinsic and synaptic homeostatic mechanisms in cortical circuit refinement. Annu Rev Neurosci. 2011; 34:89–103. [PubMed: 21438687]

Uhlhaas PJ, Singer W. Neural synchrony in brain disorders: relevance for cognitive dysfunctions and pathophysiology. Neuron. 2006; 52:155–168. [PubMed: 17015233]

Underwood JG, Boutz PL, Dougherty JD, Stoilov P, Black DL. Homologues of the Caenorhabditis elegans Fox-1 Protein Are Neuronal Splicing Regulators in Mammals. Molecular and Cellular Biology. 2005; 25:10005–10016. [PubMed: 16260614]

van de Lagemaat LN, Nijhof B, Bosch DGM, Kohansal-Nodehi M, Keerthikumar S, Heimel JA. Age-related decreased inhibitory vs. excitatory gene expression in the adult autistic brain. Front Neurosci. 2014; 8:394. [PubMed: 25538548]

Voineagu I, Wang X, Johnston P, Lowe JK, Tian Y, Horvath S, Mill J, Cantor RM, Blencowe BJ, Geschwind DH. Transcriptomic analysis of autistic brain reveals convergent molecular pathology. Nature. 2011; 474:380–384. [PubMed: 21614001]

Weyn-Vanhentenryck SM, Mele A, Yan Q, Sun S, Farny N, Zhang Z, Xue C, Herre M, Silver PA, Zhang MQ, et al. HITS-CLIP and integrative modeling define the Rbfox splicing-regulatory network linked to brain development and autism. Cell Rep. 2014; 6:1139–1152. [PubMed: 24613350]

Wu J, Akerman M, Sun S, McCombie WR, Krainer AR, Zhang MQ. SpliceTrap: a method to quantify alternative splicing under single cellular conditions. Bioinformatics. 2011; 27:3010–3016. [PubMed: 21896509]

Xie J, Ameres SL, Friedline R, Hung JH, Zhang Y, Xie Q, Zhong L, Su Q, He R, Li M, et al. Long-term, efficient inhibition of microRNA function in mice using rAAV vectors. Nat Meth. 2012; 9:403–409.

Xue M, Atallah BV, Scanziani M. Equalizing excitation-inhibition ratios across visual cortical neurons. Nature. 2014; 511:596–600. [PubMed: 25043046]

Xue Q, Yu C, Wang Y, Liu L, Zhang K, Fang C, Liu F, Bian G, Song B, Yang A, et al. miR-9 and miR-124 synergistically affect regulation of dendritic branching via the AKT/GSK3β pathway by targeting Rap2a. Sci Rep. 2016; 6:26781. [PubMed: 27221778]

Yamamoto J, Suh J, Takeuchi D, Tonegawa S. Successful execution of working memory linked to synchronized high-frequency gamma oscillations. Cell. 2014; 157:845–857. [PubMed: 24768692]

Ying Y, Wang XJ, Vuong CK, Lin CH, Damianov A, Black DL. Splicing Activation by Rbfox Requires Self-Aggregation through Its Tyrosine-Rich Domain. Cell. 2017; 170:312–323. e10. [PubMed: 28708999]

Yizhar O, Fenno LE, Prigge M, Schneider F, Davidson TJ, O'Shea DJ, Sohal VS, Goshen I, Finkelstein J, Paz JT, et al. Neocortical excitation/inhibition balance in information processing and social dysfunction. Nature. 2011; 477:171–178. [PubMed: 21796121]

Yoo AS, Sun AX, Li L, Shcheglovitov A, Portmann T, Li Y, Lee-Messer C, Dolmetsch RE, Tsien RW, Crabtree GR. MicroRNA-mediated conversion of human fibroblasts to neurons. Nature. 2011; 476:228–231. [PubMed: 21753754]

Zhao C, Sun G, Li S, Shi Y. A feedback regulatory loop involving microRNA-9 and nuclear receptor TLX in neural stem cell fate determination. Nat Struct Mol Biol. 2009; 16:365–371. [PubMed: 19330006]

Highlights

- Cytoplasmic Rbfox1 post-transcriptionally regulates Vamp1 expression
- Rbfox1 binding in the Vamp1 3′UTR antagonizes miR9-mediated repression
- Vamp1 is an inhibitory neuron-specific vSNARE enriched in Pv+ interneurons
- Vamp1 re-expression rescues the physiological defect of the Rbfox1 knockout

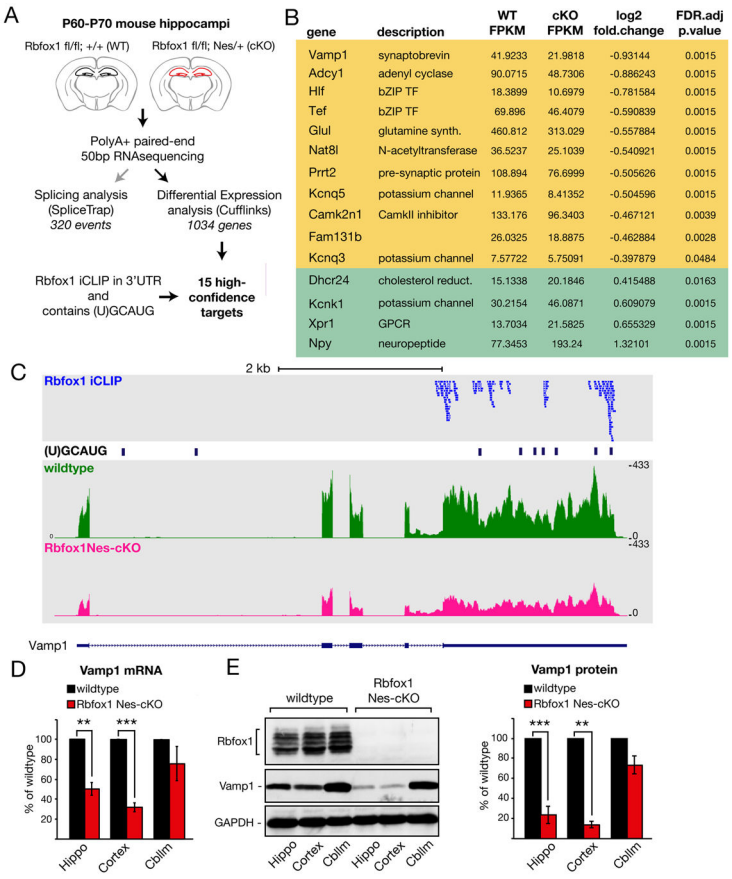

Figure 1. Vamp 1 is a direct Rbfox1 target

(A) Schematic of samples used for RNA-seq and Rbfox1 target identification. Adult hippocampi were dissected from wildtype and *Rbfox1 Nes-cKO* littermates for RNA extraction and PolyA+ mRNA sequencing. Splicing changes were analyzed using SpliceTrap and differential gene expression (DE) was detected using the Cufflinks package. Direct Rbfox1 DE targets were identified by iCLIP clusters present in two different iCLIP datasets and a (U)GCAUG within ±10nt.

(B) Table of high confidence direct Rbfox1 DE target genes filtered by the criteria outlined in (A) with down-regulated transcripts in yellow and up-regulated transcripts in green.

(C) UCSC genome browser view of mouse Vamp1 gene expression and RBFOX1 binding. Top, Rbfox1 iCLIP tags (blue) from the nucleoplasmic fraction of adult mouse brain, with Rbfox binding motifs (U)GCAUG indicated as black bars below. Middle, RNA-seq reads mapping to Vamp1 from representative wildtype (green) and *Rbfox1 Nes-cKO* (pink) hippocampi. The gene structure of Vamp1 is shown at bottom (tall boxes, exons; short boxes, 5′ and 3′ UTRs; dashed lines, introns; arrows indicate 5′→3′ direction). Genomic scalebar is shown at top.

(D–E) Vamp1 mRNA and protein levels are reduced in the *Rbfox1 Nes-cKO* forebrain but not in cerebellum. (D) qPCR analyses of Vamp1 mRNA from adult hippocampus, cortex and cerebellum of wildtype and *Rbfox1 Nes-cKO* littermates. Vamp1 was normalized to Hprt expression and shown as a percentage of wildtype in each brain region. (E) Left,

immunoblot of RBFOX1, VAMP1 and GAPDH. Right, quantification of Vamp1 protein as a percentage of wildtype expression for each brain region after normalization to GAPDH. For D, E: n=3 littermate pairs; Student's t-test; ** p≤0.01, *** p≤0.001; error bars, s.e.m. See also Figure S1 and Tables S1–4.

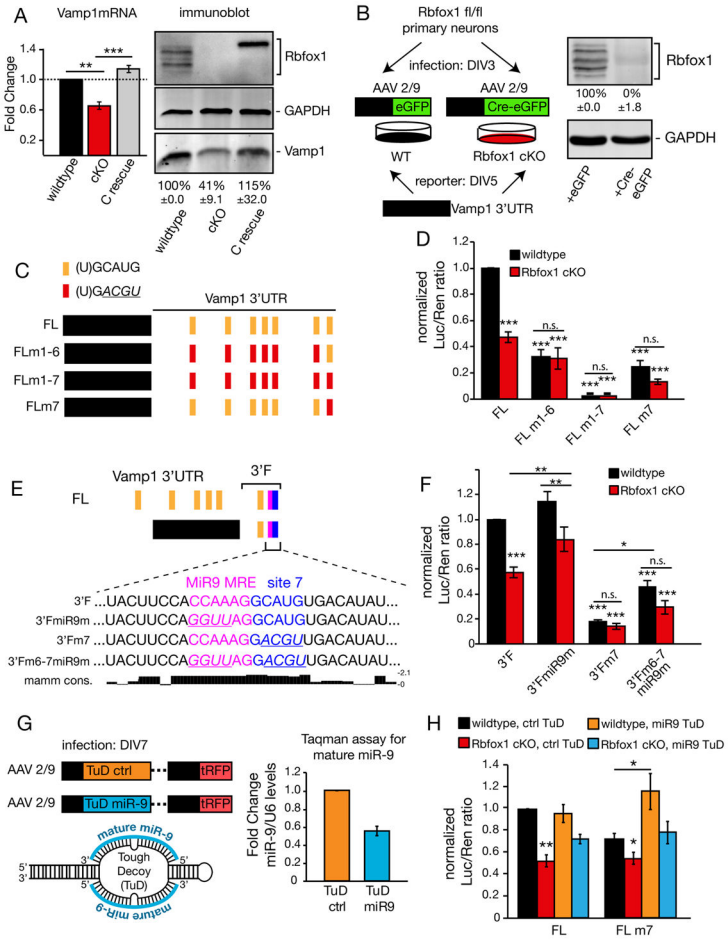

Figure 2. The Vamp1 3′UTR confers Rbfox1-dependent expression

(A) Cytoplasmic Rbfox1 rescues Vamp1 expression levels. Left, qPCR of Vamp1 mRNA in wildtype (black), *Rbfox1 Nes-cKO* (red) and cKO primary hippocampal neurons transduced with AAV2/9 *hSyn*-Rbfox1C (C rescue; gray). Vamp1 was normalized to Hprt expression levels and shown as fold-change relative to wildtype. Right, immunoblot of RBFOX1, VAMP1 and GAPDH. Average levels of VAMP1 expression normalized to GAPDH and relative to wildtype are given below Vamp1 panel. n=3 cultures (biological replicates); ANOVA with Bonferroni correction; ** p≤0.01, *** p≤0.001; error bars, s.e.m.

(B) Left, schematic of luciferase experiment. Right, immunoblot of RBFOX1 and GAPDH in DIV14 neurons transduced with *hSyn*-eGFP and *hSyn*-Cre-eGFP. Average RBFOX1 expression normalized to GAPDH and relative to *hSyn*-eGFP condition given below Rbfox1 panel. n=3 cultures (biological replicates).

(C) Schematic of full length *Vamp1* 3′UTR luciferase reporters. Vertical bars in 3′UTR represent the wildtype Rbfox binding motif (U)GCAUG (yellow) or mutated motif (U)G*ACGU* (red).

(D) Quantification of full length luciferase reporter expression. Comparisons between other conditions are noted by horizontal bars. n=6 cultures (biological replicates)

(E) Schematic of 3′F luciferase reporters. Top, the full length *Vamp1* 3′UTR is shown with the indicated 3′F reporters. Vertical bars represent the Rbfox binding motif (U)GCAUG

(yellow), 3′-most motif (blue) and 3′-most *miR9* microRNA recognition element (magenta). Inset, sequence surrounding the 3′-most *miR9* site and Rbfox motif in 3′F reporters. Bottom, mammalian conservation track for inset sequence from the UCSC Genome Browser.

(F) Quantification of 3′F luciferase reporter expression. n=3 cultures (biological replicates)

(G) Left, schematic of Tough Decoy *microRNA* inhibitors. Right, quantification of mature *miR9* levels by Taqman assay in neurons transduced with the TuD-miR9 or -control virus. *miR9* levels were normalized to the total *U6* RNA levels in each sample.

(H) Quantification of FL and FLm7 reporter expression with or without *miR9* inhibition. n=9 cultures (biological replicates).

For D, F and H: Luciferase expression was normalized to Renilla, and the Luc/Ren ratio for each condition was normalized to the wildtype reporter in wildtype neurons (first black bar). Comparisons between other conditions are noted by horizontal bars. Luciferase assays were performed at DIV14. ANOVA with Bonferonni correction; * $p \leq 0.05$, ** $p \leq 0.01$; *** $p \leq 0.001$; n.s., not significant; error bars, s.e.m.

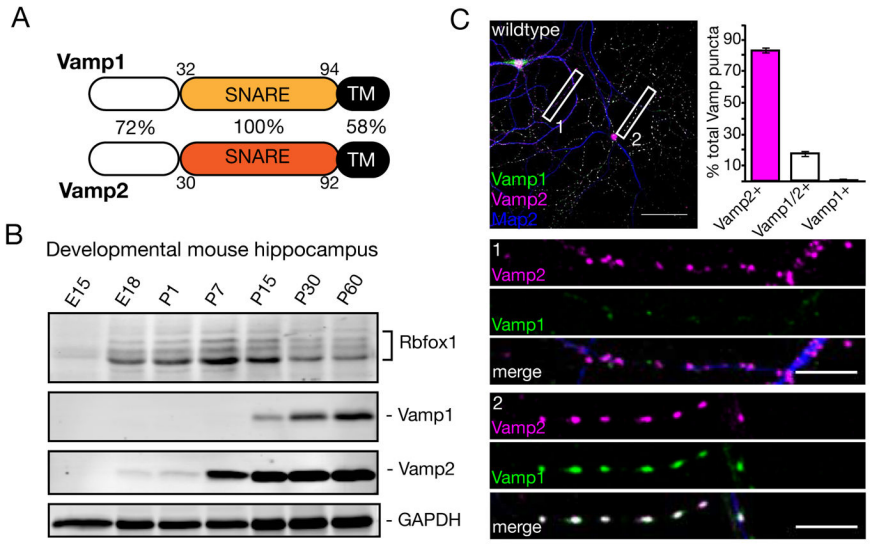

Figure 3. Overlapping and distinct expression patterns of Vamp1 and Vamp2

(A) Schematic of VAMP1 and VAMP2 protein domains. Percentages indicate level of amino acid sequence identity of VAMP1 compared to VAMP2. Numbers indicate amino acid position. SNARE, Soluble NSF Attachment Protein Receptor domain; TM, transmembrane domain.

(B) VAMP1 expression is induced late during brain development compared to VAMP2. Immunoblot of RBFOX1, VAMP1, VAMP2 and GAPDH in mouse hippocampus from E15 to P60.

(C) Left and bottom, immunofluorescence of VAMP1 (green) and VAMP2 (magenta) in wildtype DIV18 primary hippocampal neurons. MAP2, marking dendrites, in blue. Right, quantification of puncta overlaps. Right, quantification of $VAMP1^+$ and $VAMP2^+$ puncta overlap. n=3 cultures; puncta were counted in $50\mu m^2$ areas, at least 3 areas per image, in 9 images per replicate; error bars are s.e.m.; panel scalebar, 50μm; inset scalebar, 10μm; 63x magnification. See also Figure S2.

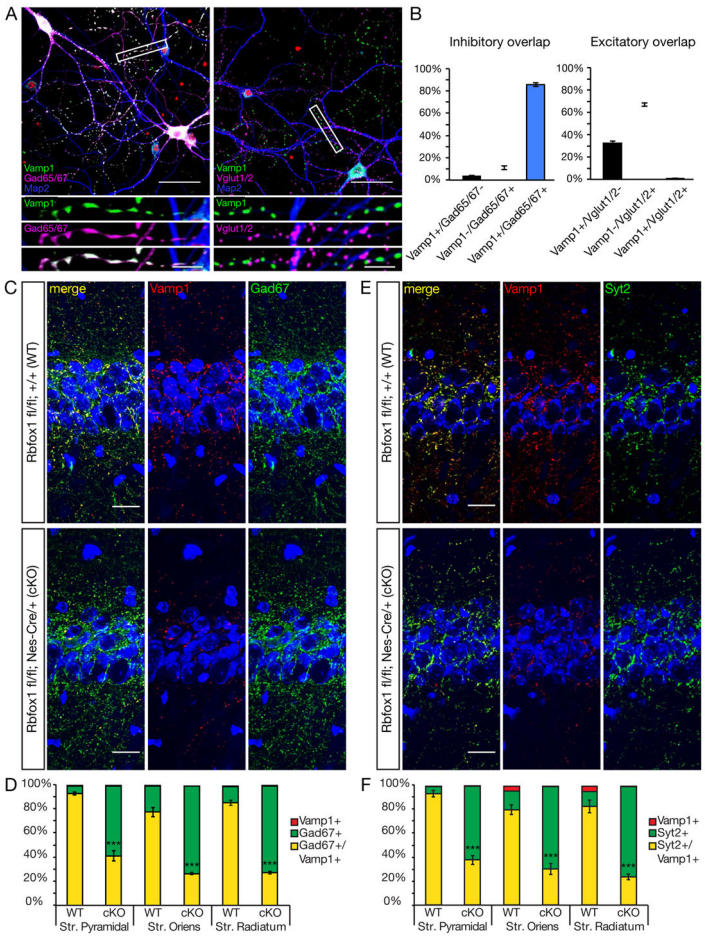

Figure 4. Vamp1 is enriched in Parvalbumin^{+} hippocampal interneurons

(A–B) VAMP1 co-localizes with inhibitory markers but has no overlap with excitatory markers.

(A) Immunocytochemistry of VAMP1 (green) and inhibitory pre-synaptic makers GAD65/67 (magenta, left panels) or excitatory pre-synaptic markers VGLUT1 and VGLUT2 (magenta, right panels) in wildtype DIV18 primary hippocampal neurons. Panel scalebar, 50μm; inset scalebar, 10μm; 63x magnification. (B) Quantification of VAMP1 overlap with inhibitory and excitatory markers. Puncta were quantified from one 100μm^2 field per image; n=15 images from 1 culture; error bars, s.e.m.

(C–D) VAMP1 co-localizes with GAD67 in the adult mouse hippocampus.

(C) Immunohistochemistry of VAMP1 (red) and GAD67 (green) in P60–P70 CA1 of wildtype and *Rbfox1 Nes-cKO* hippocampus. (D) Quantification of VAMP1^{+} and GAD67^{+} puncta in CA1. Co-localized or lone puncta are shown as a percent of all the VAMP1^{+} and/or GAD67^{+} puncta counted in each indicated area. Puncta were quantified from at least (3) 50μm^2 fields/image, from 3 images per biological replicate.

(E–F) VAMP1 is enriched in PV^{+} interneuron pre-synaptic terminals.

(E) Immunohistochemistry of VAMP1 (red) and SYT2 (green) in P60–P70 CA1 of wildtype and *Rbfox1 Nes-cKO* hippocampal sections. (F) Quantification of VAMP1^{+} and SYT2^{+} puncta in CA1. Co-localized or lone puncta are shown as a percent of all the VAMP1^{+} and

$SYT2^+$ puncta counted in each indicated area. Note that in contrast to the GAD67 IHC, in stratum oriens and radiatum a small portion (~4%) of puncta are $VAMP1^+/SYT2^-$. Puncta were quantified from at least (3) $50\mu m^2$ fields/image, from 3 images per biological replicate. For C–F, n=3 littermate pairs; ANOVA with Bonferonni correction; *** $p \leq 0.001$; error bars, s.e.m.; scalebar, 20μm; 40x magnification. Labels: **s.o.**, stratum oriens; s.p., stratum pyramidale; **s.r.**, stratum radiatum.

See also Figure S3 and Figure S4

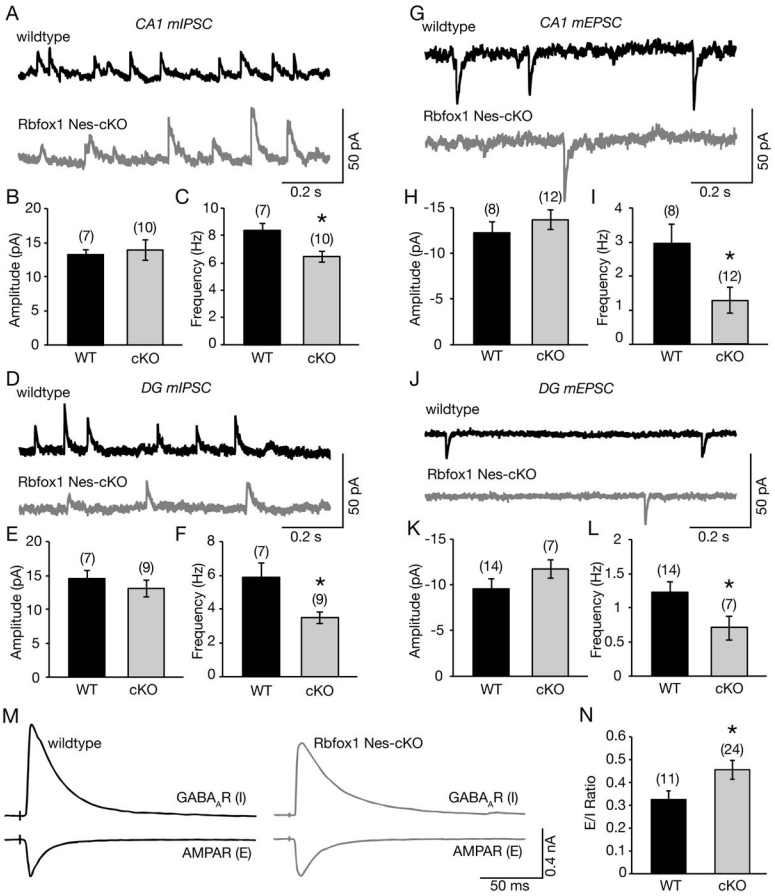

Figure 5. Inhibitory synaptic transmission is reduced in the Rbfox1 Nes-cKO

(A–F) Decreased mIPSC frequency in the *Rbfox1 Nes-cKO* hippocampus. Pan-neuronal loss of Rbfox1 leads to significantly reduced average mIPSC frequency (C, F), while average mIPSC amplitude is unaffected (B, E), in CA1 and the dentate gyrus (DG).

(G–L) Average mEPSC frequency is also reduced in the cKO CA1 (I) and DG (L); average mEPSC amplitude is not significantly affected (H, K). Sample traces are shown above quantifications.

(M–N) The E/I ratio is skewed towards increased excitation in the *Rbfox1 Nes-cKO*. Representative traces of the inhibitory $GABA_AR$ current (top trace) and excitatory AMPAR current (bottom trace) in wildtype (black) and cKO (gray) are shown in (M) with quantification in (N). The E/I ratio was measured as the ratio of the peak amplitude of each component. (N) Quantification of the E/I ratio shows that it is significantly increased in the cKO compared to wildtype. E/I currents were measured in CA1.

Number of cells recorded per condition across 3 littermate pairs is shown above bars. Student's t-test; * $p \leq 0.05$; error bars, s.e.m.

See also Figure S5.

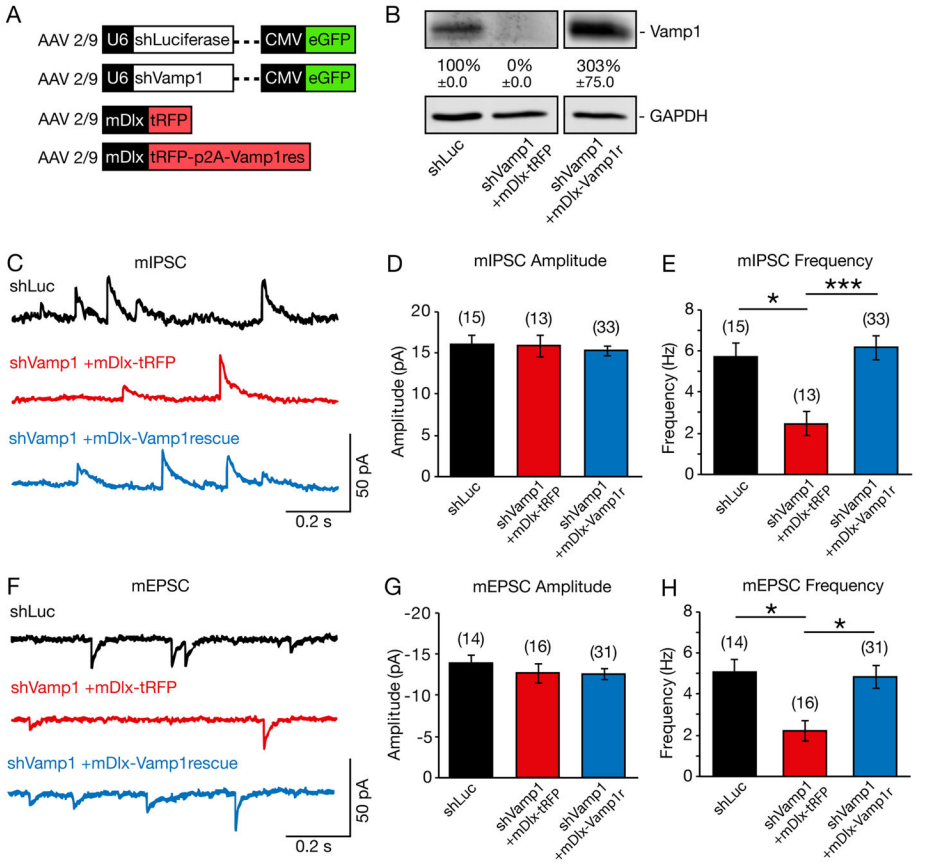

Figure 6. Vamp1 knockdown reduces inhibitory synaptic transmission

(A) Schematic of AAVs used for *Vamp1* knockdown.

(B) Immunoblot of VAMP1, VAMP2 and GAPDH neurons transduced with AAV2/9 expressing shRNA against *Luciferase* (shLuc), *Vamp1* (shVamp1) + tRFP control (*mDlx*-tRFP) or shVamp1 + Vamp1 rescue (*mDlx*-Vamp1r). Quantification of average VAMP1 expression normalized to GAPDH shown as a percentage of the control (shLuc) with s.e.m. below. n=3 cultures (biological replicates)

(C–H) Representative traces of mIPSCs (C) and mEPSCs (F) in control (shLuc, black), Vamp1 knockdown (shVamp1+mDlx-tRFP, red) and rescue (shVamp1+mDlx-Vamp2rescue, blue) treated primary neurons. Quantification of average mIPSC and mEPSC amplitude (D, G) and frequency (E, H) shown at right.

Number of cells recorded per condition across 3 cultures (biological replicates) is shown above bars. One-way ANOVA with Bonferroni correction; * $p \leq 0.05$, *** $p \leq 0.001$; error bars, s.e.m.

See also Figure S6.

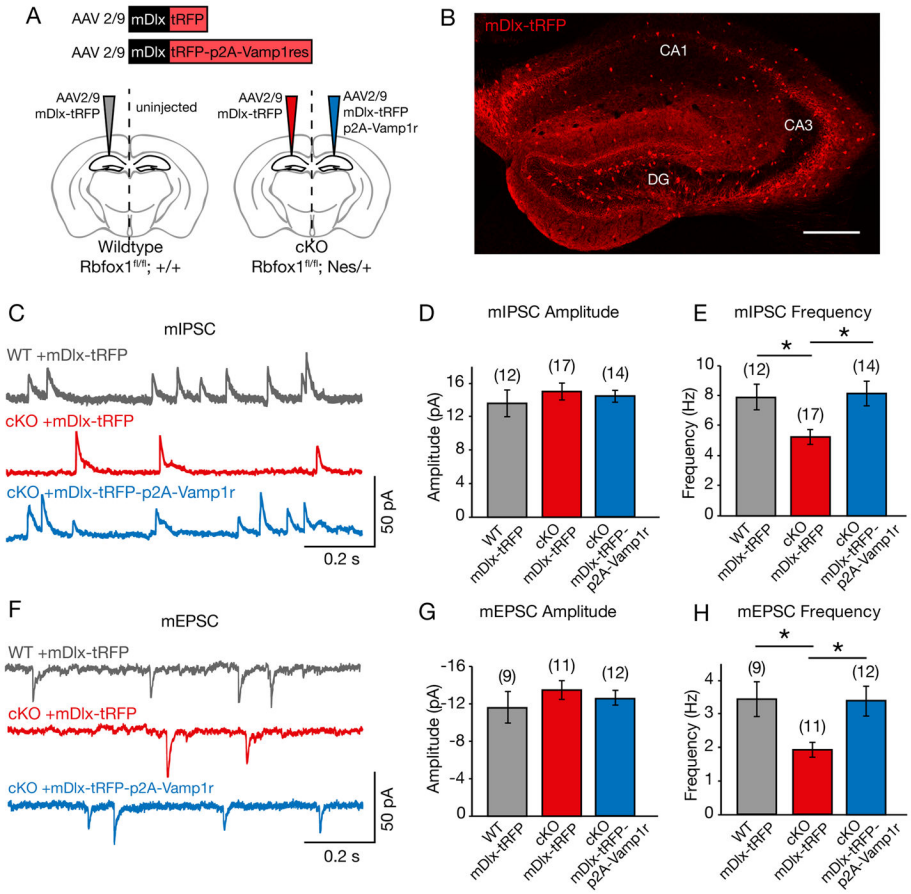

Figure 7. Vamp1 re-expression rescues inhibitory synaptic transmission in the Rbfox1 cKO

(A) Schematic of the injection experiment.

(B) Expression of AAV2/9 *mDlx*-tRFP in a representative injected hippocampus. Scalebar, 300μm; 20x magnification.

(C–E) Reduced mIPSC frequency in the Rbfox1 cKO CA1 is rescued by re-expression of *mDlx*-Vamp1.

(C) Representative mIPSC traces in the wildtype controls (WT +mDlx-tRFP), cKO (cKO +mDlx-tRFP) and rescue (cKO +mDlx-tRFP-p2A-Vamp1r) hippocampi.

(D–E) Quantification of average mIPSC amplitude and frequency shows re-expression of *mDlx*-driven Vamp1 rescues mIPSC frequency to levels similar to that of wildtype.

(F–H) Reduced mEPSC frequency can also be rescued by re-expression of *mDlx*-Vamp1.

(F) Representative mEPSC traces of samples as in (C).

(G–H) Quantification of average mEPSC amplitude and frequency shows re-expression of *mDlx*-driven Vamp1 also rescues mEPSC frequency to levels similar to that of wildtype.

Number of cells recorded per condition across 6 littermate pairs is shown above bars. One-way ANOVA with Bonferroni correction; *p≤0.05; error bars, s.e.m.

See also Figure S7.